Carbon Stardust: From Soot to Diamonds

A.G.G.M. Tielens

MS 245-6
Space Sciences Division
NASA Ames Research Center
Moffett Field
CA 94035

and
Space Sciences Laboratory
University of California
Berkeley
CA 94720

We are stardust
Joni Mitchell, 1969, Woodstock.

Abstract

This paper reviews the formation of carbon dust in the outflow from stars and the subsequent evolution of this socalled stardust in the interstellar medium. The chemical and physical processes that play a role in carbon stardust formation are very similar to those occuring in sooting flames. Based upon extensive laboratory studies of the latter, the structure and physical and chemical properties of carbon soot are reviewed and possible chemical pathways towards carbon stardust are discussed. Grain-grain collisions behind strong interstellar shocks provide the high pressures required to transform graphite and amorphous carbon grains into diamond. This process is examined and the properties of shock-synthesized diamonds are reviewed. Finally, the interrelationship between carbon stardust and carbonaceous meteorites is briefly discussed.

I Introduction

Interstellar dust is an important constituent of the interstellar medium. It absorbs efficiently visible and ultraviolet photons, which it reemits at IR wavelengths, and, thus, it regulates the spectral appearance of many dust-shrouded objects. It regulates the energy balance of the gas through the ejection of energetic electrons and gas-grain collisions. By attenuating the ambient interstellar UV radiation field, it allows (indirectly) the formation of quite complex molecules. Undoubtedly, the most abundant molecule, H_2, is formed directly on grain surfaces. The abundance of other molecules may also be influenced through grain-catalyzed reactions. Grains may also have played an important role in the cosmic history of the biogenic elements (Wood and Chang 1985). In fact, carbonaceous grains are thought to form an important component of interstellar dust (1).

In recent years, our understanding of interstellar carbonaceous dust has improved dramatically. Partly, this is a result of the opening up of the infrared

window. Infrared spectroscopy is a major tool for remote probing of the composition of interstellar dust (2). Indeed, most dust components thought to be present in the interstellar dust have been identified through infrared spectroscopy. The development of new techniques that allowed detailed analysis of microscopic amounts of stardust preserved in carbonaceous meteorites has also been instrumental in increasing our knowledge of interstellar dust (3).

The picture that arises from this new wealth of data is one where interstellar dust consists of many diverse components formed under a variety of conditions in many classes of objects. This varied background of interstellar dust makes the quotation from Woodstock particularly appropriate. A multitude of complex processes have been suggested to play a role in circumstellar dust formation and its modification in the interstellar medium. In view of the rapid developments, it has not yet been possible to weed out the unimportant processes and to concentrate on the few, more important ones. Lacking general consensus in the field, this review is an attempt to summarize my own views on these problems. Some of these seem to enjoy considerable following, others are more controversial. However, given the current large flux of ideas, any review has to be somewhat personal and dated anyway.

This review is organized as follows:

II Composition and Evolution of Interstellar Dust

Interstellar dust consists of many different components, including amorphous silicates, graphite, Polycyclic Aromatic Hydrocarbons (hereafter PAHs), amorphous carbon, icy grain mantles, and organic refractory grain mantles. Silicon carbide and magnesium sulfide, which have been identified in the outflow from carbon-rich giants and planetary nebulae might also be present in the interstellar medium. Our present astronomical knowledge on the composition of interstellar dust is summarized in table 1. For each component, this table gives the birth site(s), the fraction of the elemental abundance that it locks up, and the dust volume relative to that of the silicates. The spectral signatures that have been used to identify each dust component are also indicated. For a discussion of these the reader is referred to a recent review by us (1) as well as to earlier reviews (4,5,6).

One of the most interesting developments in recent years within the field of interstellar dust has been the realization that large polycyclic aromatic molecules form an ubiquitous component of the interstellar dust. A variety of objects show prominent emission features at 3.3, 6.2, 7.7, and 11.3 μm (5,7,8), which are characteristic of PAHs either as free-flying molecules or in the form of soot particles (9,10,11). Figure 1 compares the IR spectrum observed towards the HII region in Orion with the Raman spectrum of auto soot (11). For a highly disordered material such as soot the infrared active and Raman active vibrational modes are similar in number and frequency. It is expected that a collection of free flying PAH molecules will have a similar IR spectrum. Although it is difficult to distinguish spectrally between a collection of large PAH molecules and solid soot particles, an analysis of the excitation mechanism shows that the carrier of these emission features contains only about 20 C atoms (10,11,12). Depending on the FUV absorption properties of the particular PAHs responsible for the IR emission, about 0.5-2% of the total available elemental carbon is locked up in this component (cf., table 1). Since in many objects the IR emission originates in material recently ejected from a star, PAHs probably are the extension of the grain size distribution of circumstellar carbon grains into the molecular domain and as such may shed light on the detailed formation mechanism of carbon stardust. This will be discussed in some detail in § VI.

About half of the volume of the interstellar dust is made up of silicate grains (c.f., table 1). The other half has to be in the form of a largely carbon-bearing dust component, either graphite or amorphous carbon stardust, or organic refractory grain mantles accreted on stardust in the interstellar medium. The latter component consists of a mixed organic polymer containing CH_3, CH_2, C=O, and possibly OH groups, which is formed by UV phtolysis and (transient) heating of an icy (eg., H_2O, NH_3, CH_3OH and CO) mixture. Current observations indicate that amorphous carbon particles seem to make up only a relatively minor fraction of the interstellar dust (c.f., table 1), although this value is somewhat uncertain. From table 1, one might get the impression that the carbon dust component is dominated by organic refractory grain mantles. This is somewhat misleading. First, large graphite particles (>1000Å) do not have readily discernable absorption features and they are, thus, not accounted for in table 1. Second, the relative volume of the organic refractory grain mantles, which has presently only been detected towards the galactic center, is uncertain by a factor of about two due to the uncertainty in the precise identification of the absorbing molecules. Moreover, the relative volume of this dust component in the *local* interstellar medium may be much less. In fact, observations towards nearby stars, yield an upper limit on the relative volume of organic grain mantles which is about half that quoted in table 1. In view of these uncertainties, the distribution of

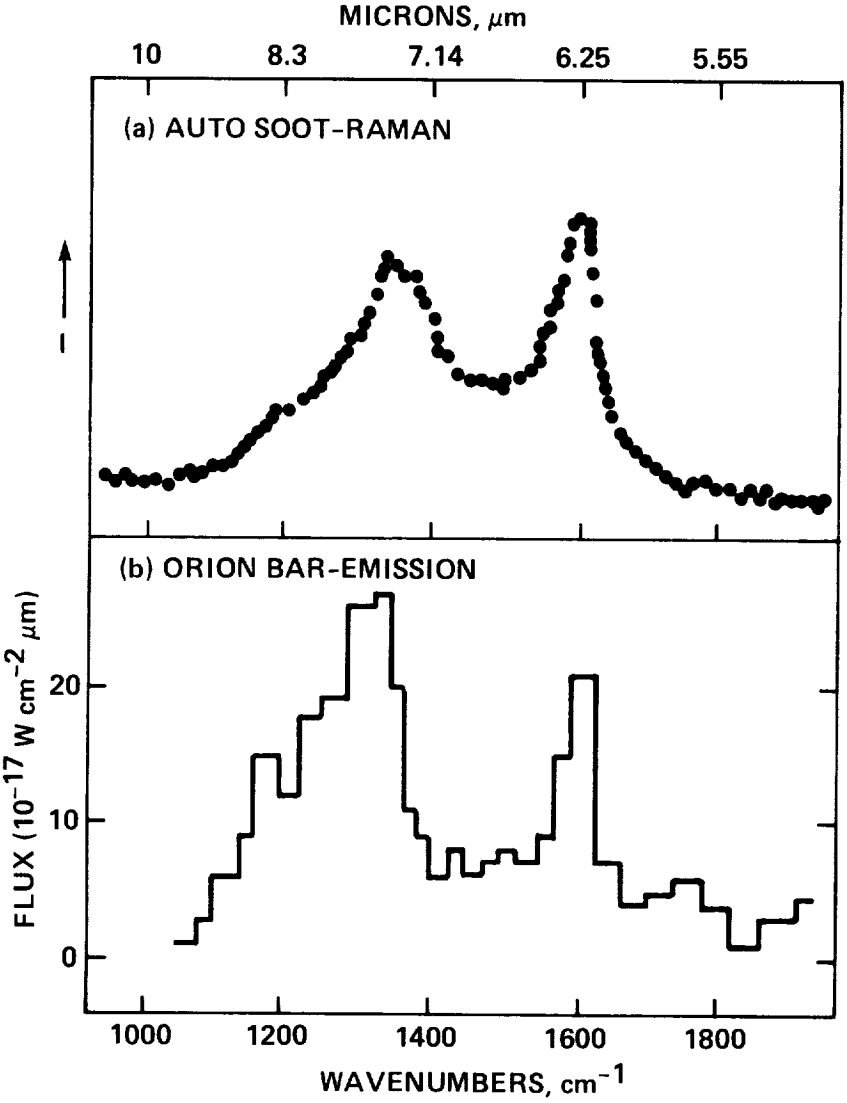

Figure 1. Comparison of the 5 to 8 μm Raman spectrum of auto soot with the emission from the Orion HII region.

Table 1: Interstellar Dust Components

COMPONENT	BIRTH SITE	ELEMENTAL ABUNDANCE[a]	REL VOL[b]	SPECTRAL SIGNATURE
Silicates	O-rich giants & Novae	100% Si 20% O (Mg & Fe ?)	1	10, 20μm features
Graphite	C-rich giants ?	>25% C	>0.25	2200Å bump[f]
PAHs	C-rich PN	1% C	0.01	3.3, 6.2, 7.7, 11.3μm emission features
Amorphous Carbon	C-rich giants, Novae, R Cr B & WC 8-10	5-10% C	≈0.1	7.6μm absorption feature ?
Icy grain mantles[d]	molecular clouds	up to 40 % C and O	up to 3	3.1, 4.6, 6.0 and 6.85μm absorption features
Organic refractory grain mantles[e]	Interstellar medium	24% C 6% O	0.8	3.4, 6.0 μm absorption features
SiC	C-rich giants & Novae	_[c]	_[c]	11.4μm emission feature
MgS	C-rich Giants & PN	_[c]	_[c]	30 μm emission feature

a) Percentage of cosmic abundance of element locked up in interstellar dust component.
b) Volume of dust component relative to that of silicates.
c) This dust component has not (yet) been detected in the interstellar medium.
d) Only observed in dense molecular clouds.
e) Only observed towards the galactic center.
f) Only graphite grains of 200Å contribute to this bump.

the carbon in the various carbon-bearing dust components in the interstellar medium should be considered approximate at this point.

Detailed models for the dust in the interstellar medium based on both premises - graphite and organic refractory grain mantles - have been developed (13-17). Using some combination of grain components, and a grain size (and shape) distribution, these models fit the visible and UV interstellar extinction curve, the linear and circular polarization, the visual extinction per hydrogen atom and, to some extent, the observed elemental depletions. Such an exercise is useful for the derivation of important quantities such as the grain size distribution within the framework of one particular model. However, these fits cannot be used to discriminate between

EVOLUTION OF INTERSTELLAR DUST

STARDUST: SILICATES, GRAPHITE, AMORPHOUS CARBON, PAHs, SiC, MgS

FORMATION PROCESSES IN CIRCUMSTELLAR SHELLS: NUCLEATION, CONDENSATION, COAGULATION

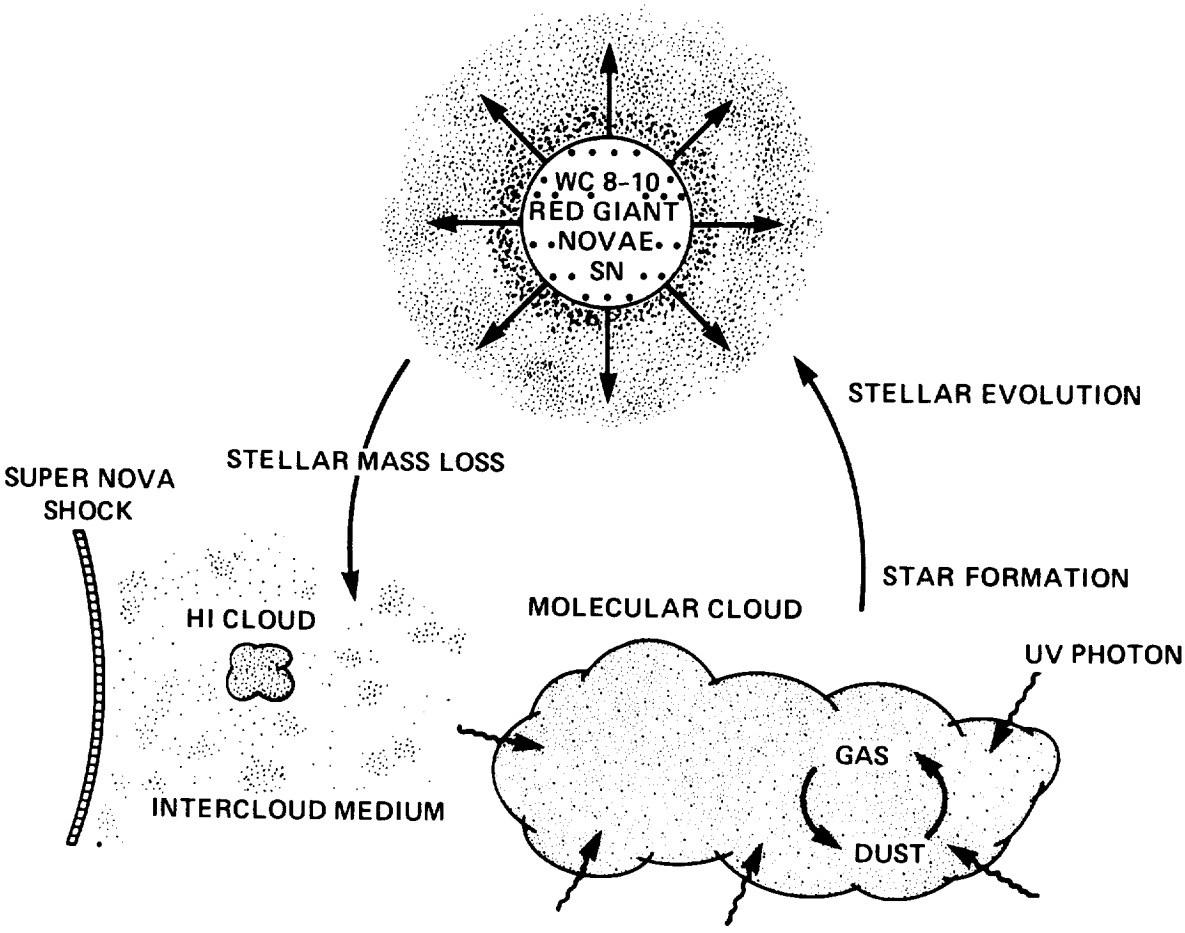

DUST IN THE INTERSTELLAR MEDIUM: STARDUST, ICY GRAIN MANTLES, ORGANIC REFRACTORY MANTLES, DIAMONDS

FORMATION PROCESSES IN MOLECULAR CLOUDS: ACCRETION, REACTION, UV PHOTOLYSIS, TRANSIENT HEATING

DUST MODIFICATION PROCESSES: (DIAMOND) METAMORPHISM AND SHATTERING IN SHOCKS

Figure 2. A schematic representation of the evolution of interstellar dust, summarizing the processes that play a role in the formation, destruction and modification of interstellar dust. Stardust is formed in the outflow from stars in the late stages of their evolution and ejected into the interstellar medium. Interstellar medium dust is formed inside dense clouds. Dust is destroyed by strong shock waves and by incorporation into newly formed stars. Grain-grain collisions in shock waves can also transform graphite (or amorphous carbon) into diamonds. See text for details.

different grain models. The visible and UV interstellar extinction curves are notably insensitive to the exact grain composition because the amorphous structure of interstellar grains as well as the presence of a size distribution tend to smear out any identifiable structure in the electronic absorption properties of the materials (1). It is because of this that widely disparate models for the interstellar dust all yield reasonably good fits to the observed interstellar extinction curve. The presence of free parameters in the models such as the shape or surface structure of the grains, which have not yet been considered in such exercises, reinforces this point.

The evolution of interstellar dust is determined by many complex, interplaying processes whose details are not understood very well. Figure 2 gives a schematic overview of the evolution of interstellar dust. Some dust components -silicates, graphite, and amorphous carbon - are formed in the outflow from stars (i.e., stardust) by nucleation, condensation and coagulation processes and their composition and sizes reflect the chemical composition and physical conditions in the condensation zones. In contrast, other dust components -icy and organic refractory grain mantles - are formed by accretion, reaction, UV photolysis, and transient heating processes in the interstellar medium (i.e., ISM dust). Prolonged processing of such grain mantles may eventually lead to the formation of a highly disordered compound consisting mainly of carbon arranged in an aromatic network. This is akin to pyrolysis of hydrocarbons and will ultimately lead to an amorphous carbon dust component. Dust is also processed in the interstellar medium by strong supernova shock waves. High velocity ion-grain collisions behind a shock will lead to sputtering, ion-implantation, and radiation damage. These will also lead to an amorphization of the surface layers. High velocity grain-grain collisions send strong pressure waves into each grain which can lead to vaporization, shock metamorphism (eg., graphite -> diamond), and shattering. Since each of these processes will lead to a different grain material, the composition of the interstellar dust in a particular region will reflect the relative importance of these processes there. *The* composition of interstellar dust is therefore in some sense a misnomer since the dust composition is expected to vary with phase (eg., diffuse ISM versus dense cloud) as well as galactic radius (eg., local versus galactic center). A global outline of the physical processes playing a role in the formation and modification of interstellar dust has been given elsewhere (2). Here we will concentrate on the formation of carbon stardust and its subsequent evolution in the interstellar medium.

III The Structure of Carbonaceous Materials

Carbon-rich materials show a wide range of behavior due to the diversity in chemical valence structure and bonding possible with carbon. These are referred to as sp, sp^2, and sp^3 hybridization, where the notation comes from the original carbon atomic orbitals involved in forming the molecular orbitals. In sp hybridization, the bond geometry is linear and two unequivalent bonds are formed, one triple and one single. An example of a simple organic compound with this structure is acetylene, H-C≡C-H. If only carbon is involved, an acetylene polymer (eg., polyynes) is formed, with a linear structure (cf., fig. 3). Note that polyacetylene is a polymer derived *from* acetylene by opening up of the triple bond and has an alternating double bond structure (eg., sp^2 bonding). In sp^2 hybridization, the bond geometry is trigonal and all the bonds lie in a plane. In general only two of the three bonds are equivalent and two single bonds and one double bond characterize this configuration. A simple organic

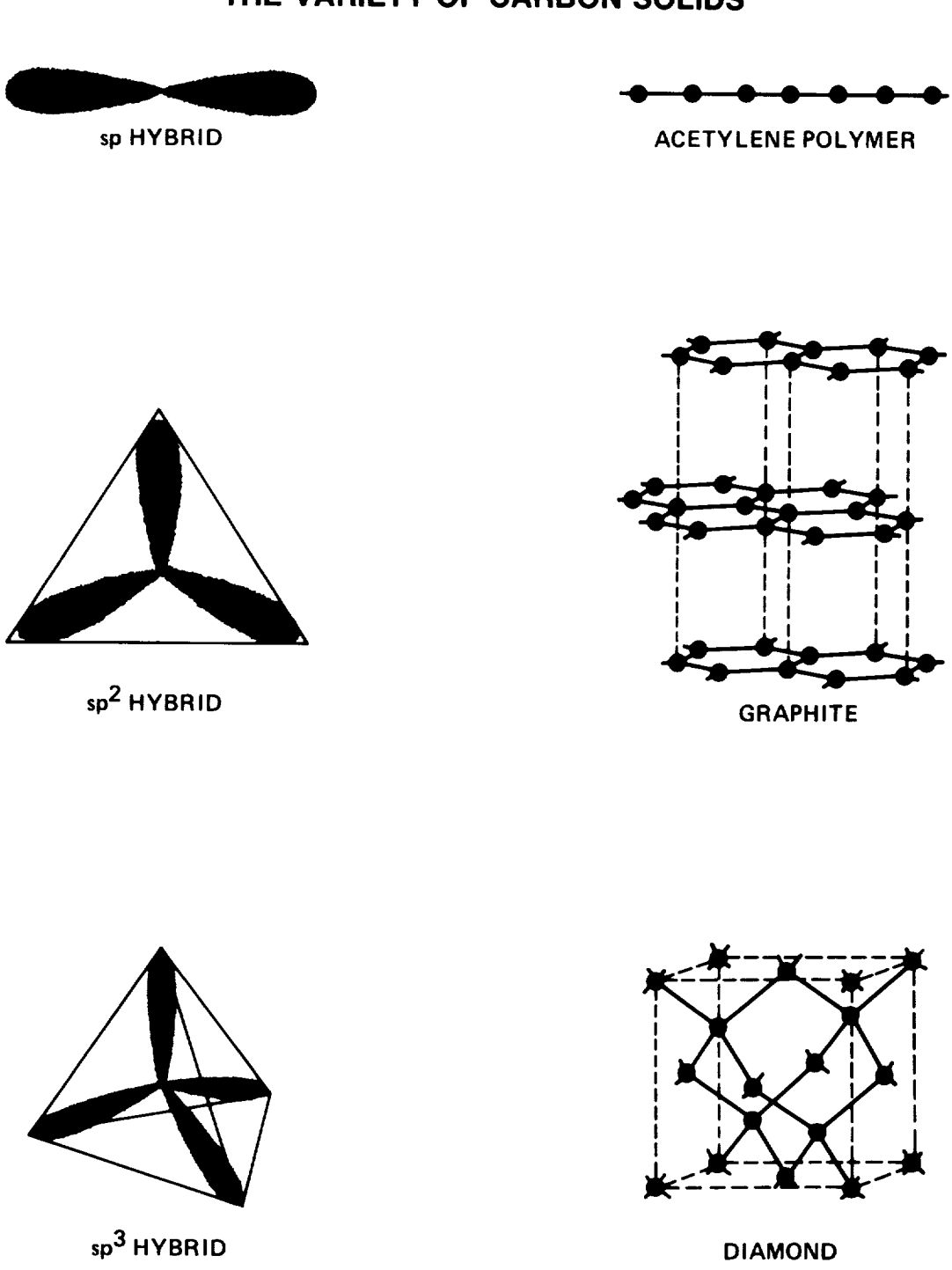

Figure 3. A schematic representation of the chemical valence structures and bonding arrangements possible with carbon. Left: the orientation of the electron clouds in the different hybridizations. Right: the corresponding carbon solids. Solid lines indicate actual bonds, while dashed lines are intended to guide the eyes. Note that sp, sp^2, and sp^3 hybridization lead to a linear, planar and three dimensional crystalline structure, respectively (see text for details).

compound with this structure is ethene, $H_2C=CH_2$. However, if only C is involved and there are enough atoms to form six-membered rings, all the bonds can become equivalent within the carbon framework. This results in an aromatic network as in graphite (cf., fig. 3). Hydrogen can bond to the external single bonds of the sp^2 carbon atoms at the periphery of the aromatic structure. PAHs are molecular examples of such structures. In sp^3 hybridization the bond geometry is tetrahedral and when only carbon is involved a diamond structure is produced (cf., fig. 3). Examples of simple molecules with this structure are methane (CH_4) and ethane (H_3C-CH_3).

Any realistic material will have some impurities, defects and dislocations and *pure* graphite, diamond or acetylene polymer materials do not exist in nature. In particular, a large variety of carbonaceous materials contain a mixture of C atoms with sp^2 and sp^3 bonding. These materials are all loosely called "amorphous carbon" in the astrophysical literature, although their physical properties can vary considerably. Hydrogenated amorphous carbon films are one example of such a mixed bonding structure and soot is another. Both materials contain large aromatic domains interspersed with tetrahedral C atoms which cross link aromatic planes. In hydrogenated amorphous carbon these tetrahedral C atoms are randomly distributed in between the aromatic C atoms. In soot they are more concentrated at the edges of aromatic planes (cf., § VIB). In both cases a large concentration of hydrogen atoms ($H/C \approx 0.1$) saturates the tetrahedrally carbon and is bonded to the edges of the aromatic domains. This difference in amorphous character is essentially that between a "truly" (random network) amorphous material and a polycrystalline material (cf., 1).

The physical and chemical properties of (hydro)carbons are largely determined by these bonding arrangements. For example, due to the conjugation of π electrons (eg., sharing of π electrons between different C atoms), graphite shows a metalic behavior within the basal (aromatic) plane (eg., graphite is a semi-metal). Its optical properties from the FUV throughout the IR are therefore dominated by interband and intraband transitions of these "free" electrons (18). When the aromatic structure is broken up by the presence of hydrogen atoms or tetrahedrally bonded C atoms, as in amorphous carbon, then the electrons will be more localized. As a result, amorphous carbon is a semi-conductor with a band gap up to 5 eV depending on the size of the largest aromatic domains. While its UV properties are still dominated by interband electronic transitions, its IR properties reflect now vibrations of the carbon (and hydrogen) skeleton (1). It should be emphasized that many of the properties of solid carbon, in particular the electronic structure, are dependent on the disorder and not the disordering agent present.

IV Carbon Injection into the Interstellar Medium

A Sources

There are many stellar sources that contribute to the carbon in the interstellar medium, including carbon-rich red giants, carbon-rich Wolf Rayet stars, and supernovae. The relative importance of these different types of objects is not well known. Even estimates of the relative importance of high mass stars versus low mass

Table 2: Stellar Mass-Loss Rates [$M_\odot$ yr^{-1} kpc^{-2}]

Object	$\dot{M}_H$[a]	$\dot{M}_c$[b]	$\dot{M}_d$[c]	Observational evidence for dust
C-rich giants	5(-4)	5(-6)	2(-6)	1) featureless continuum: amorphous carbon 2) 11.3μm feature: SiC 3) 3.3,6.2,7.7,11.3μm features (in PN phase): PAHs
O-rich giants	5(-4)	2(-6)	-	1) 10 and 20μm features: silicates
Novae	6(-6)	4(-8)	1(-8)	1) 10μm feature: silicates 2) black body (marbles ?) 3) black body + 11μm feature (SiC ?)
OB stars	1-3(-4)	1(-6)	-	1) no dust
SN: Type I Type II	- 2(-4)	3(-7) 2(-6)	- 1(-6)	1) no conclusive evidence for dust
WR stars[d]	-	4(-6)	-	1) no dust
WC 8-10	-	2(-6)	5(-8)	1) featureless continuum + 7.7μm feature: amorphous carbon (+PAHs ?)
TOTAL	1.5(-3)	1.6(-5)	3(-6)	

notes:
a) Hydrogen injection rate.
b) Carbon injection rate.
c) Carbon stardust injection rate.
d) Excluding WC 8-10 stars.

stars vary continously due to new developments in, for example, the determination of mass-loss rates (eg., IR studies) or nucleosynthetic reaction rates (eg., $^{12}C\ (\alpha,\gamma)\ ^{16}O$). Thus, while 10 years ago high mass stars (M>10 $M_\odot$) where thought to be mainly responsible for the carbon in the interstellar medium (19), in more recent studies carbon-rich red giants seem to dominate (20,21). However, there are some indications that the pendulum is swinging back into the direction of the massive stars. In the remainder of this section, estimates of the carbon mass-loss rates of different types of objects are reviewed. These estimates are summarized in table 2.

Red Giants: The mass injection rate of gas in the interstellar medium is dominated by mass-loss from red giants. A rough estimate of the total mass injection rate can be determined from the white dwarf birth rates. Assuming that each white dwarf has lost about 1 M⊙ during the red giant phase, we find from the birth rate of such objects

($\approx$1 yr^{-1}; 22) a total mass injection rate of about 1 $M_\odot$ yr^{-1}, corresponding to about 10^{-3} $M_\odot$ kpc^{-2} yr^{-1} (23). This is supported by IR and CO studies of the dust and gas mass-loss rate from these objects, which yield values between 5 and $9x10^{-4}$ $M_\odot$ yr^{-1} kpc^{-2} (21,24-27). However, estimates of the mass injection rates due to C-rich and O-rich giants separately range from equal amounts by the two types of objects (21,26) to O-rich giants dominating by a factor ten (24). The giants with a high mass-loss rate (>10^{-5} $M_\odot$ yr^{-1}) dominate the total gas return to the galaxy and the above mentioned discrepancy centers on differences in the total number of such C-rich objects estimated to be present in the galaxy. It should be noted that all studies require large correction factors for sample incompleteness and the results are thus inherently uncertain. We will adopt a return rate by C-rich giants of $5x10^{-4}$ $M_\odot$ yr^{-1} kpc^{-2}, which is about the maximum estimated (25,27). Estimates on the return rate by O-rich giants agree on approximately $5x10^{-4}$ $M_\odot$ yr^{-1} kpc^{-2} (24,27). Using these gas return rates we have estimated the C return rates (cf., table 2) by assuming an elemental C abundance of $5x10^{-3}$ and 10^{-2} by mass for O-rich and C-rich giants, respectively. The former corresponds to solar abundances, while the latter reflects the C enhancement due to dredge up of freshly synthesized material during the AGB phase (cf., § VA).

OB stars: Estimates of the total mass-loss rate of OB stars range from 1 to $3x10^{-4}$ $M_\odot$ yr^{-1} kpc^{-2} (28,29). With a solar elemental C abundance this translates into about 10^{-6} $M_\odot$ yr^{-1} kpc^{-2}.

Novae: Nova events are generally interpreted as a thermonuclear runaway in an accreting hydrogen shell on top of a degenerate C-O-white dwarf in a binary system (30). With a nova rate of 40 yr^{-1} and an ejection of 10^{-4} $M_\odot$ per event, the total mass injection rate is about $6x10^{-6}$ $M_\odot$ yr^{-1} kpc^{-2} (30). Typically H is depleted by a factor of about 3 with respect to He and little additional ^{12}C and ^{16}O have been synthesized (31-34). Assuming a C abundance of $7x10^{-3}$ by mass leads to $4x10^{-8}$ $M_\odot$ yr^{-1} kpc^{-2} for the C ejection rate (cf., table 2).

Supernovae: There is little direct observational information on the carbon injection rate due to supernovae (35) and their contribution is largely guessed at. There are two types of SN, whose only connection is the large amount of energy released ($\approx 10^{51}$ erg) and the explosive nucleosynthesis of heavy elements. Type II is generally believed to result from the gravitational collapse in massive stars ($M > 8$ $M_\odot$). Type I's are thought to be due to a thermonuclear instability of an accreting white dwarf by the accumulation of a critical mass (36). The total supernova rate has been estimated to be about $2x10^{-5}$ kpc^{-2} yr^{-1} with about equal rates for type I and II (37). The typical type II supernova has a main sequence mass of 25 $M_\odot$ of which about 2 $M_\odot$ remains behind in a neutron star (36), this yields a total H mass injection rate of about $2x10^{-4}$ $M_\odot$ yr^{-1} kpc^{-2}. Such a supernova ejects about 4 $M_\odot$ in the form of freshly synthesized heavy elements, of which 0.25 $M_\odot$ is in the form of C (36). The C injection rate from type II supernovae is then about $2x10^{-6}$ $M_\odot$ yr^{-1} kpc^{-2} (cf., table 2). This number is very uncertain since it depends critically on the somewhat uncertain ^{12}C (α,γ) ^{16}O reaction rate and its effect on the presupernova convective shell structure (36,38).

Type I supernovae will contribute much less to the galactic enrichment of intermediate-mass elements such as C. Calculations typically yield a C/Fe mass fraction ratio of about $3x10^{-2}$ of the solar ratio (39). Since about 0.5 $M_\odot$ of Fe is required to explain the lightcurves of type I supernovae (36), this implies the

production of about 2.5×10^{-2} $M_\odot$ of C per type I SN explosion. The resulting C ejection rate for type I supernovae is then about 3×10^{-7} $M_\odot$ yr^{-1} kpc^{-2}.

Wolf-Rayet stars: Population I Wolf Rayet stars are the descendants of massive ($M > 25\text{-}40$ $M_\odot$) OB stars where substantial mass-loss during the H burning phase as well as mixing processes have "uncovered" enriched stellar core material on the surfaces of these objects (40). The WC stars contain He, C and O and no evidence for H or N, while the WN have greatly enhanced He and N and no H (41). The total mass-loss rate of WC stars is estimated to be about 3×10^{-5} $M_\odot$ yr^{-1} kpc^{-2} where about 25% is due to WC 8-10, which are associated with dust formation (42). Observations of the C/He abundance ratio in these stars lie in the range 0.1 to 2 by mass (41,43), while theoretical calculations yield about 0.5 (44). Assuming a conservative value (0.2) for this ratio yields a total C injection rate of 6×10^{-6} $M_\odot$ yr^{-1} kpc^{-2} for all WC stars and about 2×10^{-6} $M_\odot$ yr^{-1} kpc^{-2} for WC 8-10. The total mass-loss rate by WN is approximately 2×10^{-5} $M_\odot$ yr^{-1} kpc^{-2} which with a C elemental abundance of about 3×10^{-4} by mass (41) translates into a negligible total C injection rate of 6×10^{-9} $M_\odot$ yr^{-1} kpc^{-2} (cf., table 2).

B) Carbon budget of the galaxy

From this discussion it is obvious that, although the mass return rate is dominated by red giants, many different object contribute substantially to the carbon budget of the galaxy. The uncertainty in these estimates should, however, once more be emphasized. While previously massive stars where thought to contribute mainly during the supernova phase (19), the upward revision in the $^{12}C(\alpha,\gamma)^{16}O$ reation rate makes this a less important source of C. Nevertheless, recent observations show that massive stars still contribute substantially albeit during the Wolf-Rayet phase. Essentially, during this phase they mix their helium-burning products to the surface and eject them in a strong wind before further nucleosynthetic burning can take place.

Elemental abundance studies of external galaxies may provide additional constraints on the type of objects that produce the C enrichment of the galaxy (45). For example, the low C/O ratios observed in the Large and Small Magelanic Clouds show that, since O is mainly synthesized in supernovae, C has to be formed mainly by other objects. Unfortunately, because of their low metalicity, the past contribution of both C-rich giants and WC stars to the elemental enrichment of these irregular galaxies has been small and thus these observations cannot be used to discriminate between these different types of stars.

The total C injection rate of 1.6×10^{-5} $M_\odot$ yr^{-1} kpc^{-2} corresponds to a C-enrichment timescale of the ISM of about 5×10^9 yrs. This may seem somewhat rapid, since the present C abundance in the ISM is very similar to the solar C abundance, which presumably reflects the C abundance in the ISM 4.5×10^9 yrs ago. However, observations allow an infal rate of unprocessed extragalactic material (eg., no heavy elements) which is equal to the H injection rate by stars (23) and this could increase the C-enrichment lifetime of the ISM by an order of magnitude.

The last column in table 2 indicates the type of dust formed in the outflow of these objects. The best evidence for carbon stardust formation is for C-rich giants. Since about half of the carbon is tied up in gaseous CO in these objects, the carbon stardust

injection rate is about $2x10^{-6}$ $M_\odot$ yr^{-1} kpc^{-2}. WC 8-10 stars also show evidence for circumstellar carbon stardust. The C fraction condensed in dust is however small ($\approx 3x10^{-2}$; 46). The contribution of these objects to the carbon stardust budget of the galaxy ($5x10^{-8}$ $M_\odot$ yr^{-1} kpc^{-2}) is thus minor. There is no conclusive evidence for dust formation in supernova ejecta (47). Assuming that half of the carbon in supernovae condenses out yields 10^{-6} $M_\odot$ yr^{-1} kpc^{-2} for these objects. There is observational evidence that suggests that some novae form SiC as well as amorphous carbon grains (48). Although silicates are not completely ruled out for the spectroscopic signatures observed, we note that studies of meteoritic carbon also strongly suggest that novae form carbon stardust (cf., § VIII). We will assume that 25% of the C condenses in the form of C stardust in novae. However, novae do not contribute much to the carbon (dust) budget of the galaxy. The total injection rate of C in solid form is then about $3x10^{-6}$ $M_\odot$ yr^{-1} kpc^{-2}, which is about 20% of the total carbon injection rate. This rather small fraction results from the large C contribution by objects which do not produce carbon stardust (eg., O-rich giants, OB stars), the small fraction of C condensed in the outflows from WC stars, and from the substantial fraction of C locked up in CO in C-rich giants. It should also be emphasized that the dust formed by supernovae and WC stars is ejected at high velocities ($\approx$1000 km s^{-1}). Appreciable destruction of this newly formed dust may take place during deceleration and mixing into the ISM due to sputtering and grain-grain collisions.

C) The ^{13}C budget

It is of some interest to examine the ^{13}C budget of the galaxy also. Here the situation is much less confused, since He burning does not produce much ^{13}C. As a result supernovae and WC stars contribute negligibly to the ^{13}C budget of the galaxy. Again C-rich red giants can be very important. The $^{12}C/^{13}C$ ratio in those objects with the largest outflows (eg., IRC 10216) is typically 45 (49,50). The ^{12}C injection rate (cf., table 2) translates then into a ^{13}C mass-loss rate of 10^{-7} $M_\odot$ kpc^{-2} yr^{-1}. For O-rich giants and OB stars a solar $^{12}C/^{13}C$ ratio is appropriate (=89), which leads to an injection rate of $3x10^{-8}$ and 10^{-8} $M_\odot$ kpc^{-2} yr^{-1}, respectively. The ejecta from novae are expected to be characterized by profoundly non-solar isotopic abundance patterns for the light elements C, N and O (30,51). Novae may indeed be an important source of ^{13}C. Calculated $^{12}C/^{13}C$ ratios range from 0.1 to 0.5 (52,53). Adopting 0.2 leads to a ^{13}C mass-loss rate from novae of $2x10^{-7}$ $M_\odot$ kpc^{-2} yr^{-1}. The total ^{13}C injection rate is then about $3x10^{-7}$ $M_\odot$ kpc^{-2} yr^{-1}.

This corresponds to an average ^{13}C mass abundance in the ejecta of $1.3x10^{-4}$, which is about 4 times solar. Again infall of metal-poor extragalactic material seems to be required to prevent rapid enrichment of the ISM. The $^{13}C/^{12}C$ ratio in the injecta is about 0.02, which is about twice solar. As a result the $^{13}C/^{12}C$ ratio in the ISM will slowly ($\tau \approx 2x10^{10}$ yrs) increase compared to solar abundances. This comparison is independent of the (uncertain) infall rate of metal-poor extragalactic material. Actually, observations of the $^{12}C/^{13}C$ ratio in the interstellar medium indicate an enrichment by about a factor 2 since the solar system formed ($\approx 4.5x10^9$ yrs; 54). However, since this enrichment timescale result from a comparison of two uncertain injection rates, this difference with observations may not be too worrysome. Observational studies of the $^{12}C/^{13}C$ ratio as a function of galactic radius may be a very valuable tool in unraveling the contributions of different types of objects to the carbon budget of the galaxy. Preliminary observations indicate that there is no evident gradient in the $^{12}C/^{13}C$ ratio in the solar neighborhood (55). This is somewhat surprising in view of the large contribution of "pure" ^{12}C by WC stars, which show a

marked increase in surface density in the direction of the galactic center (42). This should be contrasted with the more even distribution of white dwarfs (eg., red giants descendants) and novae, which contribute most of the ^{13}C. This might indicate that red giants actually dominate the carbon budget (56). We do note, however, that the O/H gradient in the galaxy is also fairly small (57) despite the large contribution from massive stars to the O budget and this argument may not be conclusive.

V The Dust Condensation Zone

We will consider three different types of objects, characterized as carbon-rich (eg., C/O>1), losing mass and showing evidence for dust formation. These are C-rich red giants, R Coronae Borealis (R Cr B stars), and late-type, carbon-rich Wolf Rayet stars (WC 8-10). Well studied prototypes of these stellar classes are IRC 10216, R Cr B itself and Ve 2-45, respectively. Each of these classes represents late stages in the evolution of stars of different mass (and evolution). C-rich giants are low mass stars ($M<8\ M_\odot$) which have been (slightly) enriched in carbon through the dredge up of freshly synthesized material. The evolutionary status of R Cr B stars is not well understood. Presumably, these low mass stars ($\approx 1\ M_\odot$) have lost most of their H envelope due to H processing through the CNO cycle and possibly explosive ejection of their envelope and are now underway from a red supergiant stage to a white dwarf stage. These objects are very rare and have therefore been neglected in the C budget of the galaxy. As discussed in § IV, Wolf-Rayet stars are an advanced stage in the evolution of massive OB stars ($M>25\ M_\odot$), where He burning products are exposed at the surface. Table 3 lists typical parameters for these prototypes and their circumstellar envelope. These have been compiled from the recent literature (41-43, 58-63). It should be emphasized that most of the parameters reported actually show a considerable spread within each class. A few of the reported parameters need some further clarification.

A) The photosphere

The stellar radii have been calculated from the luminosities assuming that the stellar spectrum can be represented by a black body at the effective temperature, T_{eff} ($R_* = [L_*/4\pi\sigma]^{1/2}\ T_{eff}^{-2}$, where σ is Stefan-Boltzman's constant). The total pressure in the photosphere, P_{tot}, refers to the depth where the continuum emission originates. For the C giants it has been taken from model calculations (65) for log g=1. For the R Cr B stars it has been estimated assuming hydrostatic equilibrium and the Rosseland mean opacities appropriate for these stars (66). The total pressure in the photosphere is not a very meaningful concept for Wolf-Rayet stars where the continuum emission originates from a region well into the outflow and, thus, the stellar radius (defined this way) actually falls beyond the sonic point of the outflow (42).

The observed C/H and C/O ratios for an optically selected sample of C-rich giants are typically about 6×10^{-4} and 1.1, respectively (67). However, for our purposes the high mass-loss stars, which have been selected against in this sample, are of more interest. The quoted values seem reasonable and are also in agreement with abundances derived for planetary nebulae (58,67). The $^{12}C/^{13}C$ ratio depends strongly on the amounts of He burning shell and equilibrium CNO cycle material mixed into the

Table 3: Physical Conditions in the Carbon Dust Condensation Zone

Type	C-rich Giant	R CrB	WC 8-10
STELLAR PARAMETERS			
L_* ($L_\odot$)	10^4	10^4	10^5
T_{eff}(K)	2500	7000	20000
R_*($R_\odot$)	530	67	25
P_{tot}(dyn cm^{-2})	4 (3)	3 (3)	--
Period (days)	200	40	--
C/H	6 (-4)	300	--
C/He	7 (-3)	3 (-2)	8 (-2)
C/O	1-2	2	[10][a]
$^{13}C/^{12}C$	3 (-2)[b]	<2 (-2)	[0][a]
CIRCUMSTELLAR SHELL: CONDITIONS AT THE CONDENSATION RADIUS			
M_{tot}($M_\odot$ yr^{-1})	1 (-5)	1 (-6)	3 (-5)
v_∞ (km s^{-1})	15	200	1500
R_c (R_*)	5	10	500
T_d (K)	≈1000	≈1000	≈1000
T_g (K)	≈800	-	-
P_{tot} (dyn cm^{-2})	6 (-5)	3 (-6)[c]	3 (-8)[c]
P_{carbon} (" ")	4 (-8)	1 (-7)[c]	2 (-9)[c]
T_{exp}/T_{col}	500	40[c]	2[c]
observed composition	molecular (see table 4)	C, C_2, CN	C^+, C^{2+}, C^{3+}, C

notes:
a) These abundance ratios refer to theoretical calculations rather than observations.
b) This ratio varies widely from object to object within the range 3.5-100.
c) These numbers have been calculated assuming a spherically symmetric outflow and the actual densities and pressures may be much higher (see text).

atmosphere by the dredge up process during the helium shell flash at the tip of the asymptotic giant branch (68). Observed values range from 3.5 to 100 (ie., solar). The value shown for IRC 10216 (cf., table 3) seems to be typical for high mass-loss C-rich giants (49).

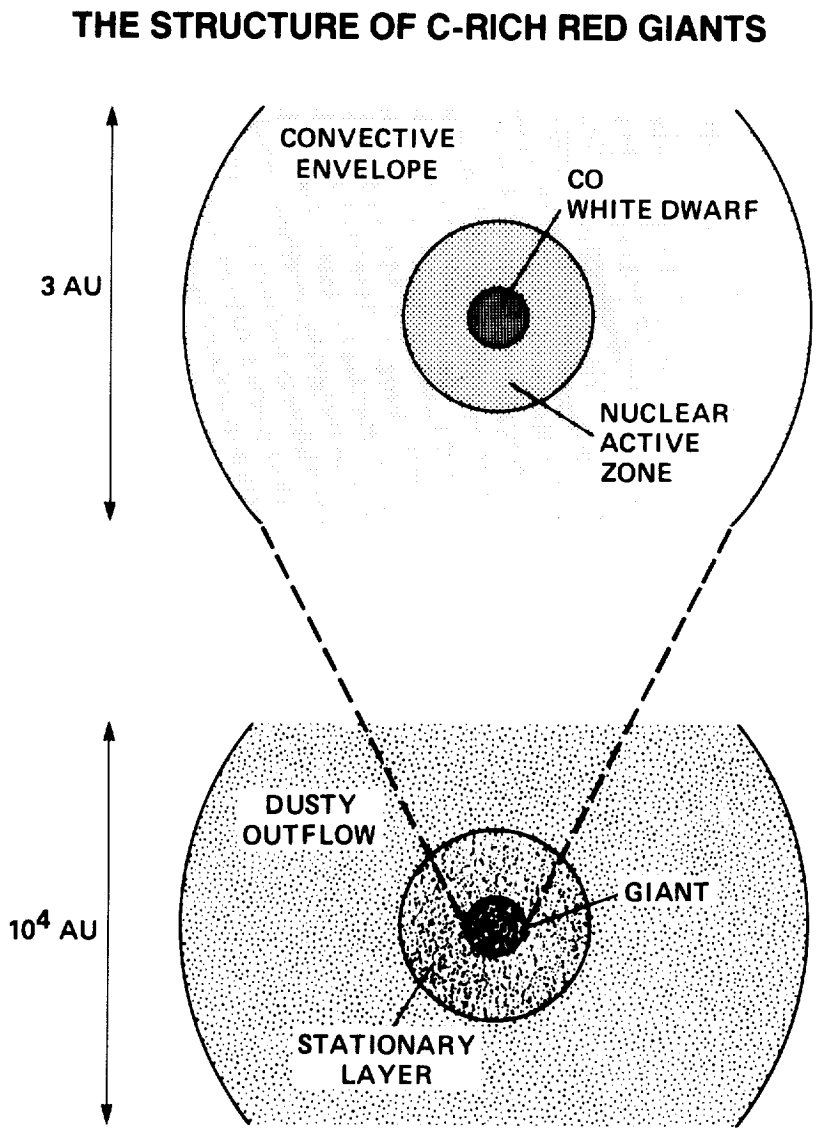

Figure 4. A schematic representation of the structure of red giants (top) and their surrounding circumstellar shells (bottom). 1 AU is the sun-earth distance$\approx 1.5 \times 10^{13}$ cm. For clarity the various inner zones are not drawn to scale. A star on the asymptotic giant branch consists of a central, carbon-oxygen, white dwarf ($\approx 10^{-3}$ AU) surrounded by a thin shell - in which nuclear burning takes place - and an extensive, convective envelope. Strong shock waves in the photosphere transport matter to large distances ($\approx 5R_*$) where dust condensation takes place (stationary layer). Radiation pressure on the dust accelerates the dust outwards and the gas is dragged along.

B) Structure of the outflow

A star on the asymptotic giant branch (AGB) has exhausted its hydrogen and helium nucleosynthetic fuel in the core, but is not massive enough (<8 $M_\odot$) to explode as a supernova (type II). The core then collapses into a carbon-oxygen white dwarf ($\approx 10^9$ cm), which is surrounded by a nuclear active zone in which alternately hydrogen and helium burns (cf., fig. 4). This core and nuclear active zone are embedded in an extensive ($\approx 5 \times 10^{13}$ cm) convective envelope (68). The envelope is unstable and pulsations drive strong shock waves into the photosphere, transporting matter to large distances from the stellar surface. This material forms a (quasi) stationary layer at about 5R_* ($\approx 2 \times 10^{14}$ cm), where solid dust particles condense out. Radiation pressure on these dust grains leads then to the formation of an extensive ($\approx 10^{17}$ cm), expanding ($\approx$10 km s^{-1}) dust shell. The gas is collisionally coupled to the dust and is dragged along. During the last part of this evolutionary phase of a low-mass star when the mass of the convective envelope becomes small ($\approx 10^{-3}$ $M_\odot$) a fast, low density wind (ie., "superwind") from the white dwarf compresses the surrounding gas and dust shell, which is ionized by UV photons from the white dwarf. The AGB star and its surrounding shell has become a planetary nebula. The nuclear fuel is exhausted and the white dwarf will eventually cool into oblivion. During the penultimate phase, some planetary nebula nuclei develope atmospheric characteristics of carbon-rich Wolf-Rayet stars (ie, population II WC stars; 69).

The mass-loss of population I Wolf-Rayet stars (ie., M_*>20 $M_\odot$) is due to radiation pressure on atomic lines. Dust forms only at large distances from the stellar surface and, in contrast to red giants, plays no dynamic role in the outflow. These radiation driven winds from Wolf-Rayet stars are highly unstable and strong shocks are expected to develop (42). Velocity amplitudes may be as large as 500-1000 km s^{-1}. For dust formation, the most important effect of these instabilities is perhaps the development of dense pockets of gas which can shield the budding molecule and soot formation processes from the disruptive effects of stellar and shock-produced UV photons. Indeed, the small fraction of C condensed in the form of dust and the absence of IR variability suggest that dust formation occurs in a large number of highly localized, dense regions in the outflow. The increase in dust mass towards later-type WC star is then attributed to a larger number of such regions, caused perhaps by a larger susceptibility to this instability.

In R Cr B stars, ejection from the pulsating stellar photosphere seems to take place in periodic, extremely dense, but localized, "puffs". During the expansion the temperature in these ejected gas blobs drops and dust is formed (62). Due to the localized nature of the ejection process, the stellar disk is only sporadically covered, giving rise to ocassional deep minima in the observed light curves of these objects. Dust condensation takes therefore place at much higher densities than derived from the nominal mass-loss rates assuming spherical outflow at the terminal velocity.

C) Physical conditions in the dust condensation zone

IR observations of the vibrational transitions of CO show that C-dust condensation in red giants takes place at a relatively large distance from the stellar photosphere ($\approx 5R_*$; 63). This is in agreement with IR speckle measurements, which show similar innner shell radii (58). For R Cr B and WC stars the condensation radius has been estimated from the condensation temperature assuming reasonable absorption

properties for the dust (64,70). The derived inner radius for the WC stars is in good agreement with IR speckle studies of Ve 2-45. For red giants the gas temperature at the condensation radius is measured to be about 800 K (63). No measurements for WC and R Cr B stars are available. The total and partial carbon pressures, P_{tot} and P_C, at the condensation radius have been determined from the mass-loss rate, the outflow velocity (eg., $\rho = \dot{M}/[4\pi R_c^2 v_\infty]$) and the (gas or dust) temperature. As remarked above, because of clumping, these values may not be very relevant for R Cr B and WC stars.

It is obvious from table 3 that carbon dust formation occurs under a wide variety of conditions. The effective temperature of the central star, for example, ranges from 2500 to 20000 K and this will have a profound influence on the chemical composition of the expanding shell (cf., below). The elemental composition of the outflow also varies dramatically from mainly hydrogen to mainly helium and carbon in the three classes of objects. However, dust formation always seems to occur at a condensation temperature of about 1000 K. An important parameter to consider in dust formation studies is the ratio of the expansion timescale, τ_{exp}, to the collision timescale, τ_{col} (71). The expansion timescale is approximately given by R_c/v_∞ (cf., table 3). Anticipating the discussion in § VI, dust formation is initiated by collisions with the most abundant, carbon bearing, gas phase molecule. For C-rich giants this is acetylene and, assuming a typical neutral-radical reaction rate (2×10^{-11} cm^3 s^{-1}), the calculated ratio is embarrassingly small (cf., table 3). This implies that kinetic effects (eg., activation barriers) are extremely important and that the dust formation process may be far from thermodynamic equilibrium. Essentially, the dust formation process has to be extremely efficient and should occur upon collision. Although grain growth probably occurs at this rate, such a high efficiency is difficult to understand for the initial nucleation step, which is probably inhibited by considerable activation barriers. On the other hand formation of the initial condensation nuclei (eg., PAHs; see § VI) in or slightly above the stellar photosphere, will be inhibited by the strong shock waves traversing this region (72). This presents an enigma for any stardust formation theory. It has been argued that the observation of a stationary layer and the IR speckle results are perhaps not in direct conflict with dust nucleation starting in the photosphere (58). Indeed, small PAH nuclei possess a large electronic band gap (cf., § III) and will not experience much radiation pressure until they have grown to about 50Å. Their dynamic influence on the outflow is therefore small. Likewise, if only a small fraction of the carbon is locked up in these species, they will not be detected in the IR (unless a bright FUV source is present as in planetary nebulae). The observations do imply, however, that further growth to dust particles is inhibited until about $5R_*$ above the photosphere. Since nucleation is the bottleneck to dust formation (further growth of nuclei into large dust grains is expected to be rapid), these observations do indirectly constrain nucleation to the stationary layer.

D) Chemical composition

The last row of table 3 summarizes the chemical composition in the outflows from these objects. For R Cr B stars only a few very simple carbon-bearing species have been observed. The winds from WC stars are completely ionized. The abundance of neutral carbon is about 10^{-6} of the elemental carbon abundance in these stars. A wide variety of molecular species have been observed in C-rich late type giants. These are summarized in table 4. This data again refers specifically to the outflow from the well-studied C-rich giant, IRC 10216 (73-76). The IR observations refer to pencil beam observations against the IR stellar and dust continuum and are thus heavily weighted towards the high density region close to the star. Molecular abundances can

Table 4: Molecular Composition of Outflow from C-rich Giants

I. Infrared Observations[a]			II. Radio Observations[b]	
Species	N_i [cm^2]	X_i	Species	N_i [cm^2]
CO	2.0(20)	6(-4)	HCN	1.(16)
C_2H_2	3.0(18)[c]	9(-6)	HC_3N	3.(15)
HCN	>1.5(18)	>5(-6)	HC_5N	6.(14)
NH_3	1.0(17)[d]	3(-7)	HC_7N	3.(14)
CH_4	1.8(16)	5(-8)	HC_9N	2.(14)
SiH_4	4.0(15)	2(-7)	$HC_{11}N$	2.(14)
C_2H_4	4.0(15)	1(-8)	CH_3CN	4.(12)
CS	6.0(19)	2(-4)	CN	9.(15)
			C_3H	1.(14)
			C_4H	3.(15)
			C_5H	1.(14)
			C_6H	2.(14)
			C_3N	1.(15)
			C_3H_2	2.(14)
			SiC_2	2.(15)
			SiO	1.(16)
			SiS	7.(15)
			H_2S	1.(13)
			CS	4.(15)
			C_2S	1.(14)
			C_3S	1.(14)
			NaCl	5.(12)
			AlCl	5.(12)[e]
			KCl	5.(12)[e]

notes:
a) Data taken from the compiliation in reference (73). Abundances calculated assuming a CO/H_2 abundance of $6x10^{-4}$.
b) Data taken from references (74-76).
c) 600K C_2H_2 with N= 2.0(19) also present.
d) Cooler (<200K) NH_3 also observed.
e) Column densities assumed to be equal to that of NaCl.

be derived from the measured column densities, assuming a size scale (ie., the inner radius). The radio studies, in contrast, are dominated by the cooler, less dense material at large distances from the star. Since the observed intensity measures the total emiting volume, the column densities derived from the radio observations depend critically on the assumed (ie., unknown) inner radius (74). No direct comparison is therefore possible between the two sets of column densities given in table 4.

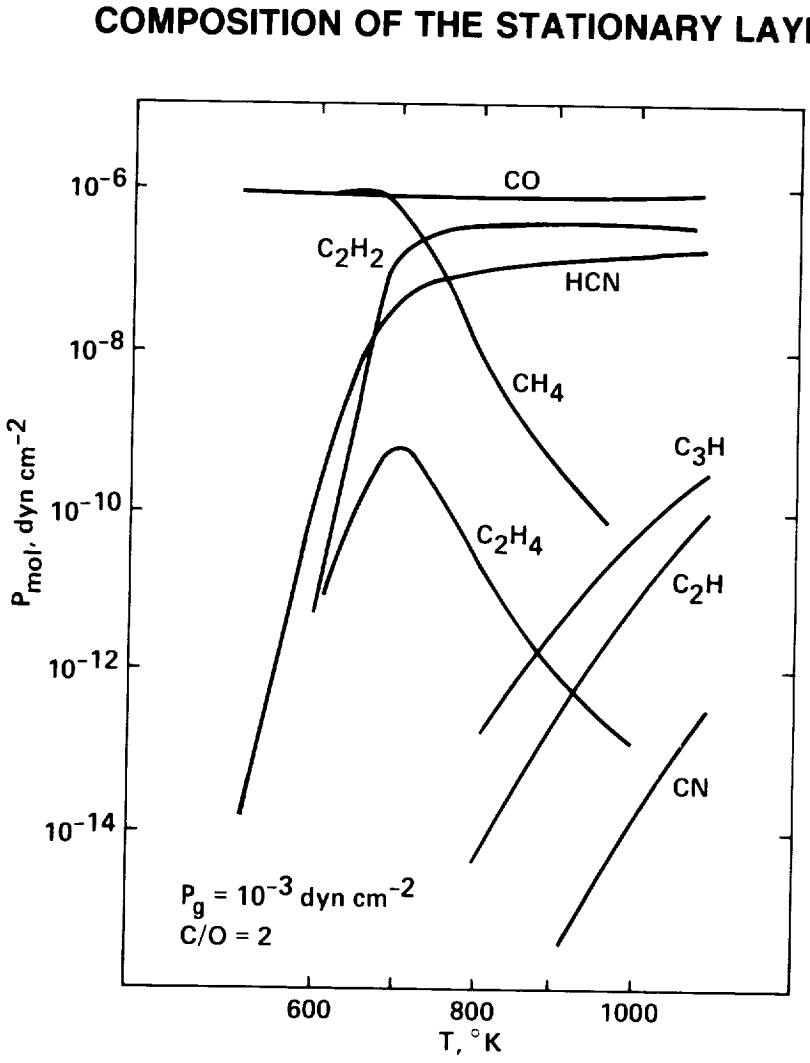

Figure 5. The chemical composition of the stationary layer calculated assuming thermodynamic equilibrium (adapted from reference 63).

A strikingly rich variety of molecules has been observed in IRC 10216, much more than in any other circumstellar shell. To a large extent, this is probably due to its proximity to the sun (d≈200pc) and other C-rich envelopes are likely to be as chemically diverse. The molecules in table 4 can be divided in four categories: 1) Simple and stable molecules expected in a C-rich environment (eg., C_2H_2, HCN, CH_4, C_2H_4; see below). 2) A series of acetylenic chains (cyanopolyynes; eg., HC_3N, HC_5N). 3) A series of reactive radicals (eg., C_3H, C_4H). 4) A set of molecules involving S, Si and Cl. This diversity reflects the large number of chemical processes, which are of importance in circumstellar envelopes. These include (nearly) thermal equilibrium processes in the stellar photosphere and inner envelope, shock processes, UV photochemical processes, grain condensation and grain surface reactions (61). All of these can influence the chemical composition of the dust condensation zone. Figure 5 shows the abundance of some simple carbon bearing molecules as a function of gas temperature, calculated assuming thermal equilibrium at a total gas pressure of 10^{-3} dyn cm^{-2} and a C/O ratio of 2 (63). This pressure is perhaps a little higher than expected for the dust condensation zone in C-rich giants (cf., table 3). At high temperatures, most of the carbon is locked up in CO and C_2H_2. At lower temperatures, CH_4 becomes important and even some of the CO is converted, which results also in an increase of the abundance of other O-bearing molecules (eg., SiO, H_2O; 63). Besides acetylene, attention should be drawn to the relatively high abundance of C_2H at high temperatures, which may play a key role in carbon dust condensation (cf., § VI). Note that these calculations ignore the dust condensation process. Similar calculations have been performed including dust condensation (again assuming thermal equilibrium), but for a high pressure ($P_{tot} = 10^3$ dyn cm^{-2}) more appropriate for the stellar photosphere rather than the condensation zone (77). Moreover all of these calculations ignore chemical kinetics which
certainly plays an important role in determinig the molecular composition and ultimately carbon dust formation (cf., § VI). Finally, atomic H may also play an important role in soot formation. H_2 is the most abundant molecule in these equilibrium calculations and atomic H is a trace species. However, shocks driven into the extended photosphere by the stellar pulsations in red giants may actually lead to H_2 dissociation and the H/H_2 ratio may be far from equilibrium since H_2 reformation will be slow under these conditions (78).

VI Chemical Pathways to Carbon Stardust

In this section we will discuss the formation of carbon dust in the outflow from carbon-rich objects. We will concentrate on C-rich giants, since they dominate the carbon stardust budget (cf., § IV) and since the physical conditions in their outflows are much better determined than those in WC stars or R Cr B stars. Moreover, their chemical composition resembles that of sooting flames and we can draw on an immense chemical literature on soot formation under such conditions (79). Some of the differences that can be expected to be important in other objects will be pointed out.

A) Thermodynamics and carbon condensation

Most studies of stardust formation are based on thermochemistry, which considers the condensation of solids out of a (slowly) cooling gas that originally contained no solids (71,80). The "condensation" sequence is then determined based on

THERMODYNAMICS OF CARBON DUST FORMATION

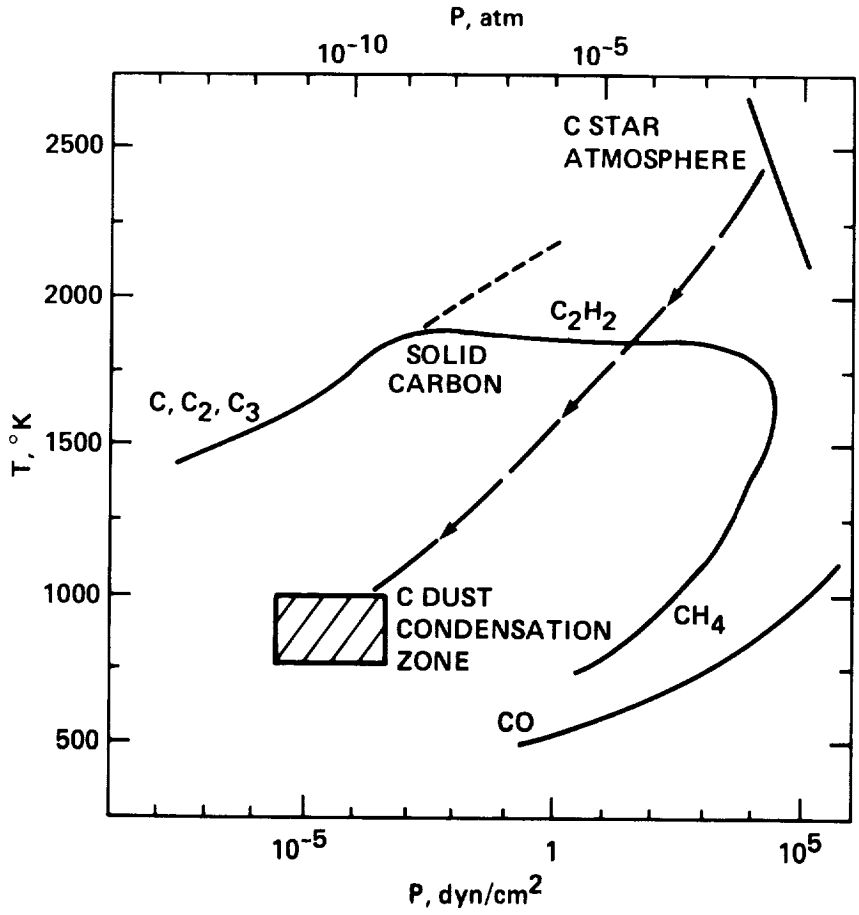

Figure 6. The phase diagram appropriate for C-rich red giants (adapted from reference 80). The line labeled solid carbon encloses the regime in which graphite is stable. Surrounding it, the position of the various, stable, carbon-bearing gas phase molecules are shown. To the left (right) of the dashed curve hydrogen is mainly atomic (molecular). The solid line in the lower right hand corner deliniates the transition from the CO to the H_2O dominated regime. The conditions appropriate for the photospheres and dust condensation zones of C-rich giants are also indicated. Due to the presence of strong shocks, the actual path of a cooling gas element in the outflow is far more complex than indicated. See text for details.

thermodynamic equilibrium. Essentially, the free energy of many atoms, molecules and solids are used to derive their relative abundances in equilibrium. Condensation sequences have been published for many different pressure, temperature, and elemental abundance regimes (71,80-82). Figure 6 shows the result for a C-rich (and H-rich) atmosphere (80). The thick solid curve encloses the regime where graphite is stable. Outside of it gas phase carbon species are more stable. Their relative abundance depends on the total (H) pressure. At the lowest pressures C, C_2 and C_3 are most important. Between 10^{-3} and 10^4 dyn cm^{-2} acetylene dominates, while at high pressures CH_4 ties up the carbon (80). To the left (right) of the dotted curve atomic H (H_2) is most abundant. The conditions appropriate for the photosphere and the condensation zone in C-rich giants are also schematically indicated (cf., table 3). As expected from observations (59) the conditions in the stellar photosphere correspond to the acetylene dominated regime. Carbon stardust formation occurs in a regime where graphite is thermodynamically favored (cf., fig. 6). The long-dashed line schematically indicates the path of a cooling and expanding gas element. The actual path is, however, much more complex, due to the strong shocks traversing the extended photosphere (cf., § VB). Nevertheless, condensation does not seem to take place immediately upon passing the solid carbon stability line. The flow is, thus, highly supersaturated when the grains actually condense and an amorphous rather than crystalline material will form (cf., 1). The thermodynamic stability curve for such a material is, however, expected to be very similar to that of graphite (83). This late onset of condensation may reflect the importance of kinetics (eg., time-dependent nucleation) as well as other non-equilibrium effects.

The actual grain growth process is generally calculated using classical homogeneous nucleation theory (80,84). This assumes that the abundance of a cluster containing N atoms can be derived from the monomer concentration using the free energy of this cluster. The latter is often derived from the experimentally measured, bulk surface tension (84), although this may lead to large errors for small clusters (85). For small clusters, the surface free energy makes a large contributions to the total free energy. As a result, below a critical cluster size (which depends on the degree of supersaturation), clusters are more likely to evaporate than to grow. Statistical fluctuations are then responsible for producing clusters larger than this critical size, which can then grow on to actual dust grains (83,84). The formation of the critical cluster forms thus a bottleneck in the dust grain nucleation. Typical the final number of monomers in a grain is then approximately given by $[\eta/\ln(\eta)]^{1/3}$ (80), where η is the number of monomer collisions within a relevant timescale (ie., τ_{exp}/τ_{col}). For the conditions in C-rich red giants (cf., table 3) this results in $N \approx 5 \times 10^5$ or a particle size of about 100Å. Since the initial steps are expected to be associated with considerable activation barriers, the actual grain size will be much smaller. This small expected grain size reemphasizes the dust nucleation problem alluded to in the previous section.

Chemical reaction rates are, to a large extent, governed by kinetic rather than thermodynamic factors, a point which has largely been ignored in stardust condensation studies. In particular, nucleation theory was developed for the formation and growth of liquid droplets where the bulk surface tension is more accurately known than for solid clusters. Indeed, the concept of a "surface" (or surface tension) is not even well determined for small molecular clusters (85) and such reasoning can easily lead to erronous results. For example, it has been argued that, if the surface free energy of tetrahedrally-bonded carbon clusters is equal to

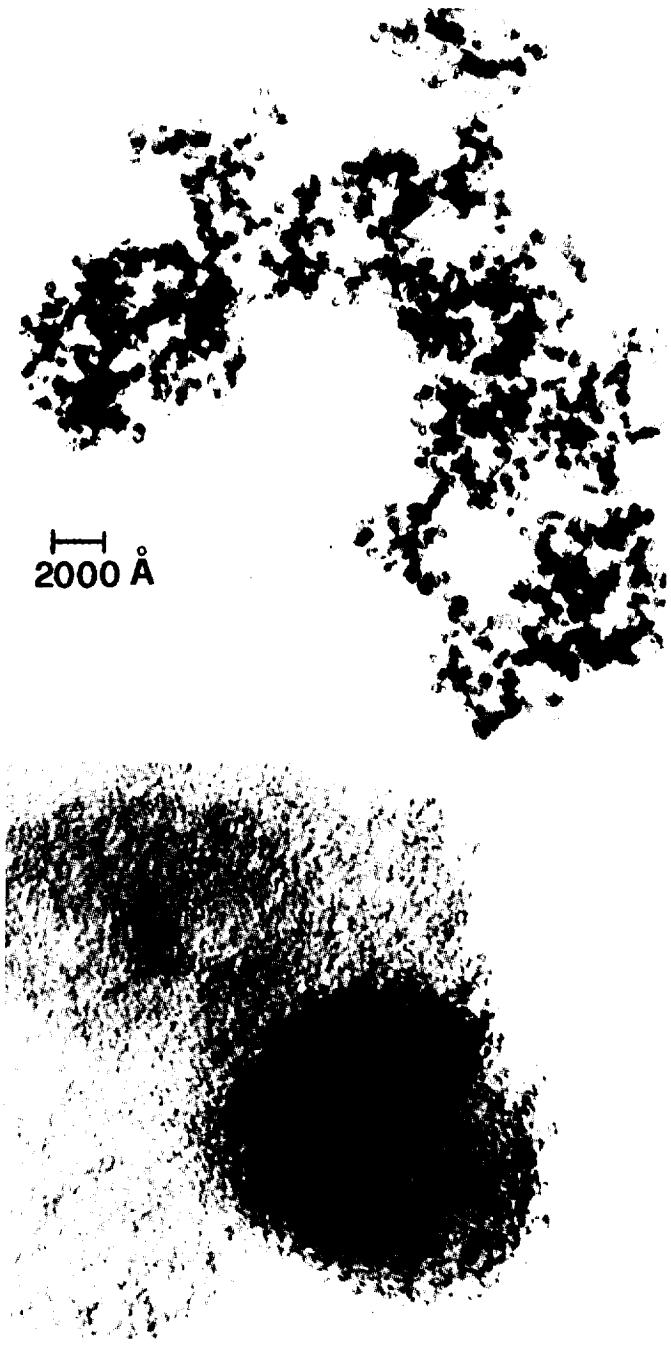

Figure 7. Transmission Electron Microscope photographs of a typical amorphous carbon sample produced by striking an arc between two carbon electrodes (courtesy of reference 92). Top: Carbon necklace. Bottom: a single grain.

that of aromatically-bonded clusters, diamond clusters would be favored over graphitic clusters in the carbon condensation route around stars, essentially due to the difference in volume density (86). However, aromatic clusters grow at the periphery of the aromatic planes and the surface free energy is associated with the dangling bonds of these peripheral carbon atoms. In contrast, diamond clusters grow three dimensionally. As a result the number of "surface" carbon atoms and their associated dangling bonds per carbon atom in the cluster is much larger in a "diamond" cluster than in a "graphite" cluster. It is only at high pressures, where volume plays a dominant role, that the high volume density of diamond favors diamonds over graphite. As a result aromatic clusters (eg., PAHs, see below) are expected to form around stars in agreement with astronomical observations and with laboratory studies of soot formation.

Although one may attempt to circumvent this problem in the definition of the cluster surface free energy in one way or another (84), the application of classical nucleation theory to stardust condensation is even more fundamentally flawed. In particular, the monomers (eg., atomic C) out of which graphite or amorphous carbon has to be formed do not even exist, as such, in the outflow from C-rich giants where most of the elemental carbon is in the form of CO and C_2H_2 (87). A similar argument holds also for the condensation of silicates around O-rich giants. For a meaningful assesment of carbon dust formation, the chemical pathways which convert these molecules into solid dust grains has to be identified (79,88).

B) Soot formation

The processes that convert C_2H_2 into carbon grains in the outflow from C-rich red giants are probably very similar to those occuring during the gas phase pyrolysis of hydrocarbon molecules. There is an extensive literature on soot formation in combustion environments, in a large part driven by concerns on internal combustion engine efficiency, pollution, and health hazards (cf., 89-91 and references therein). Here we will briefly summarize the salient points.

Soot is a general side product of the combustion and pyrolysis of hydrocarbons. Morphologically, soot is independent of generation method and fuel type. Transmission electron microscopy shows that soot particles consist of a large number of small (100-1000Å) spherical particles arranged like pearls on a chain. Figure 7 shows a typical example generated by striking an arc between two amorphous carbon electrodes (taken from 92). Similar results are obtained when burning hydrocarbons such as methane, acetylene or benzene in air at room temperature and in pyrolysis studies in shock tubes and flow reactors (89-95). These particles are made up of microcrystallites with sizes in the range 10 to 25Å. X-ray analysis shows that the carbon atoms are arranged in a graphitic planar structure and thus such microcrystallites resemble large PAH molecules. Indeed, smaller members of the condensed aromatic ring compounds (eg., PAHs) are readily extracted from soot particles using organic solvents. Although the microcrystalline planes are parallel to each other, they are more randomly stacked in soot particles than in graphite (95).

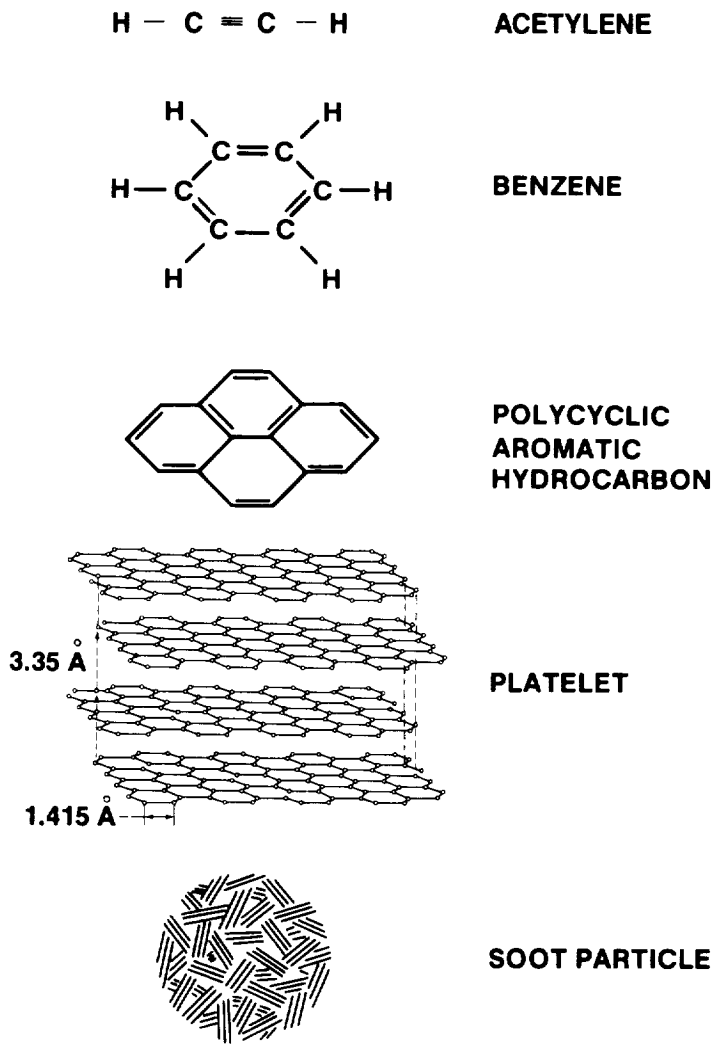

Figure 8. The structure of the various molecules and particles involved in one possible carbon stardust formation scheme. Acetylene is the precursor gas phase molecule. Various chemical processes convert these molecules into benzene molecules. Further chemical growth involving acetylene leads to the formation of large polycyclic aromatic hydrocarbons. Several of these planar molecules stacked together form a platelet. These platelets are the building blocks of soot particles. These platelets as well as the layers within them are generally cross-linked by tetrahedrally bonded carbon atoms and chains (see text for details).

The chemical nature of the soot can vary within a flame. When first formed, the particles contain a large number of hydrogens (C/H≈1, when a≈50Å), which are distributed in between the aromatic layers. ESR studies show that these small particles have a pronounced free radical character and they continue to grow through surface reactions. Both the hydrogen content (C/H≈0.1) and radical nature decreases during this growth. At a size of about 200 Å rapid surface growth stops and the particles aggregate in larger grains.

Three distinct steps can thus be discerned in the formation of soot (89-91): 1) the breakdown of fuel molecules to precursor molecules which react rapidly to form larger species; 2) chemical growth that results in the formation of numerous small particles (a>10Å); and 3) particle growth by surface reactions as well as by clustering and agglomeration. In flames these processes compete with oxidation processes. In the outflow from C-rich red giants, however, the C/O ratio is larger than 1 and essentially all of the oxygen is tied up in CO. In other words, all of the available carbon has already been burned in the stellar photosphere and the conditions resemble those of a fuel-rich flame. Thus, while the incandescent soot particles in flames, which give rise to its characteristic yellow color, will typically burn up quickly in the air at the top of the flame, this oxidation process will be of no importance in C-rich giants.

C) PAHs and the formation of carbon stardust

The critical intermediates in the carbon condensation route have to be highly stable against dissociation and yet posses a high reactivity towards polymerization. Several different chemical pathways to soot formation have been proposed based on neutral radicals, ions, PAHs, polacetylenic chains, or Buckminsterfullerene as intermediaries (89,90,96,97). The high tendency of aromatic fuels to soot, the high stability of PAHs as well as their structural similarity (the aromatic C backbone) has led to the notion that PAHs are the building blocks of soot particles. In the case of C-stardust formation around C-rich giants, the importance of PAHs is underscored by their ubiquitous presence in C-rich planetary nebula (7). Following references (79,88), we will identify PAHs as the key intermediates in C-stardust formation in these objects. The basic steps in soot formation in this scheme are schematically shown in figure 8. As remarked above, other pathways have been proposed in which PAHs are unreactive sidebranches (ie., dead-ends), and the following discussion should be considered illustrative rather than authorative. Moreover, as will be discussed in § E, it is likely that in different environments different mechanisms dominate C-stardust formation.

In the outflow from carbon-rich giants, acetylene and its radical derivatives are likely to be the precursor molecules from which soot is formed and the soot-limiting step is the formation of the first aromatic ring (cf., fig. 8). Rapid chemical growth of this ring then forms larger PAHs. At some stage clustering of PAHs becomes important and small platelets are formed in which small PAHs are randomly stacked. Simultaneously, further chemical growth will take place, in particular at the periphery of the aromatic planes. This may lead to cross-linking of the planes by tetrahedrally bonded carbon. Some crosslinking may also occur randomly dispersed in the aromatic planes. Finally, these platelets can cluster to form a spherical soot particle (cf., fig 8). In flames, these spherical soot particles cluster further to form a "pearl-like" necklace (cf., fig. 7).

THE CHEMICAL PATHWAY FOR CARBON DUST FORMATION

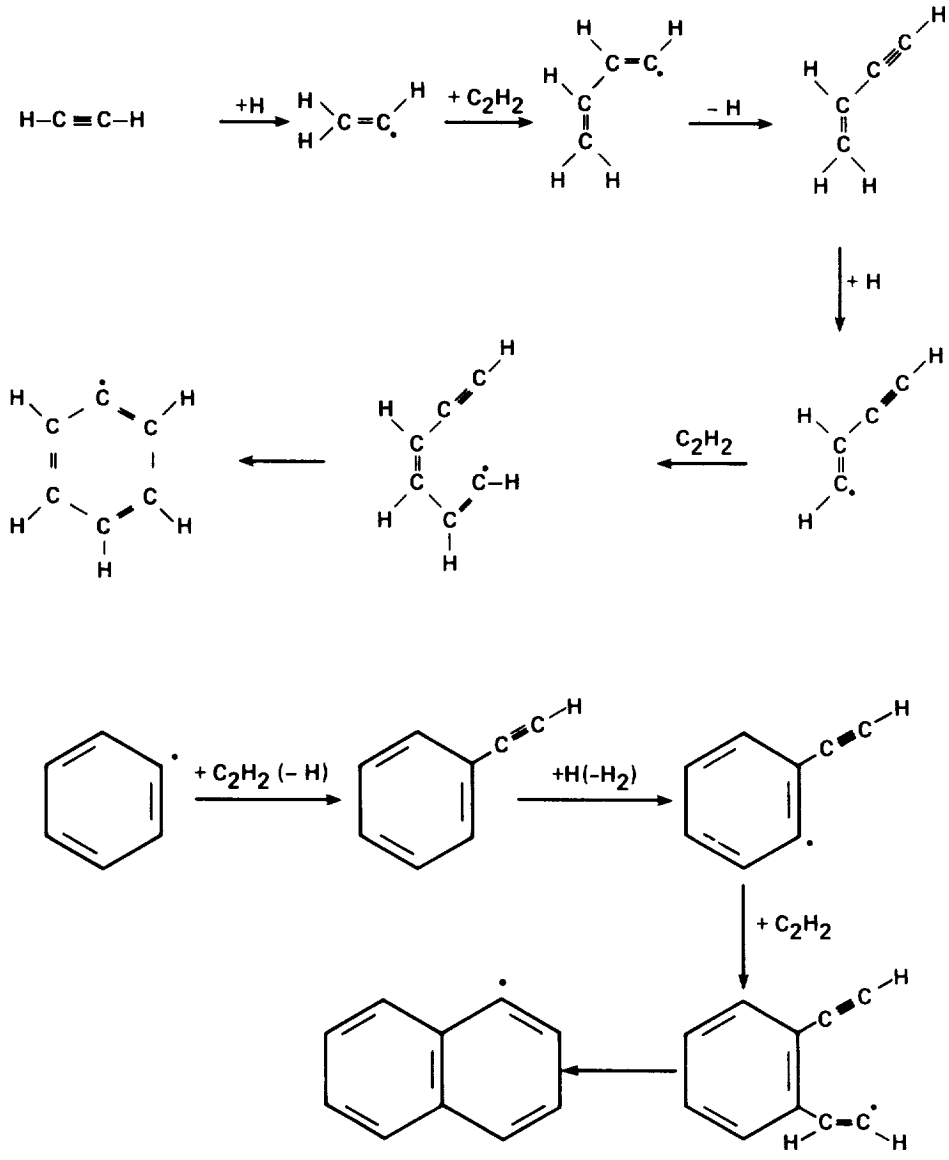

Figure 9. One possible chemical pathway towards soot (adapted from reference 103). Top: the formation of the first aromatic ring, starting from acetylene. Bottom: further chemical growth takes place through alternating steps of radical site formation and acetylene addition. Branching reactions have been omitted for clarity (see text for details).

The temperature and pressure history of a parcel of gas in the outflow of a carbon-rich giant is very complex due to the strong shock waves propagating through the extended photosphere which lead to large temperature and density excursions. Dust formation will then occur far above the photosphere ($R \approx 5R_*$) where the activity generated by the shock waves has died down (72). PAH formation in flames starts typically when the temperature drops below about 2000K (98). The temperature of the extended red-giant photosphere is not determined by radiative equilibrium but by shock passage. A postshock temperature of 2000K corresponds to a shock velocity of a few km s^{-1} and shock calculations in Mira atmospheres indeed indicate a typical distance of about $5R_*$ above the photosphere (99-102).

Figure 9 shows the first steps in one possible chemical pathway to soot derived from detailed kinetic model studies of shock-tube pyrolysis of acetylene at about 1700 K (78, 79, 103). A very similar cyclization model has been proposed to explain measured product distributions in sooting laminar flat flames with a variety of hydrocarbons (104). Many different branching reaction pathways are possible at all of the intermediate steps. For clarity, these have been ignored, since theoretical studies indicate that they are of lesser importance. There are two steps in this reaction scheme: a series of reactions describing the formation of the first ring out of acetylene and one describing further chemical growth. Formation of the first aromatic ring forms a bottleneck for the soot yield. It is started through the formation of the ethynyl radical (C_2H) through H abstraction. This radical can then attack the triple bond in another acetylene molecule and react to form C_4H_5. Two steps of H abstraction by H atoms, followed by reaction with yet another acetylene yields C_6H_5. Cyclization of this radical via interaction of the unpaired electron with the triple bond leads then to the first aromatic ring. Once the first ring is formed subsequent chemical growth consists of (more or less) alternating steps of the formation of a radical site through H atom abstraction, acetylene addition and cyclization. This is illustrated for the formation of the small PAH, naphthalene. Further chemical growth will take place through the fused PAHs pyrene, coronene, and ovalene (105).

The stable molecular intermediates, including phenylacetylene (C_4H_4), acenaphthalene ($C_{12}H_8$) and the pericondensed PAH pyrene ($C_{16}H_{10}$), present in this reaction scheme play an essential role. The reactions leading from one radical to another are reversible at these temperatures and quickly set up an equilibrium distribution. The reactions leading to these stable intermediates, however, are irreversible and thus "pull" the reaction sequence towards molecular complexity and soot formation. The importance of pericondensed aromatic hydrocarbons, such as pyrene, coronene and ovalene, in this scheme rest mainly in their high thermodynamic stability, resulting from their maximum resonance energy and minimal stress energy (105). The enthalpy of formation can also be maximized by minimizing the entropy change by returning as many H_2 molecules as possible to the gas phase. This favors molecules with an as short as possible boundary structure and may actually lead to (smaller) aromatic molecules having pentagons or squares in their carbon skeleton (78). The molecule cyclopentanaphthalene is an example of this latter principle. The stresses due to the presence of pentagons in the carbon skeleton will lead to warping of the intrinsically planar structure of PAHs. If present in an ordered fashion this can even result in spheroidal molecules such as Buckminsterfullerene (C_{60}; 106), which are closed upon

Table 5: The most abundant PAHs in flames[a]

Species	formula	abundance[b]
Naphthalene	$C_{10}H_8$	100
Acenaphthalene	$C_{12}H_8$	100
Phenanthrene	$C_{14}H_{10}$	30
Pyrene	$C_{16}H_{10}$	30
Benzo[g,h,i]fluoroanthene	$C_{18}H_{10}$	10
1,12-Benzperylene	$C_{22}H_{12}$	3
Coronene	$C_{24}H_{12}$	1
Soot[c]	--	1000[d]

notes:
a) Taken from (98) and references therein.
b) Mass abundances in the burned gas normalized to coronene.
c) Typical soot diameter ≈250Å, corresponding to about 10^5 C atoms.
d) Measured when chemical growth has stopped. However, further physical growth (ie., clustering) may increase this ratio further.

themselves and do not contain any hydrogen. When present in a disordered fashion, pentagons will lead to a curling of the aromatic planes without actual reconnection (96,97). However, cyclopenta groups are relatively unstable and may be partially lost along the reaction pathway (103). Whether they will persist in the carbon condensation route probably depends on the relative importance of thermodynamic and kinetic considerations.

Table 5 list some typical PAHs detected in sooting flames with an estimate of their relative abundance (98). In the case of well-controlled combustion mainly the thermodynamically most stable PAHs are formed and survive in the burned gas. Although the absolute amount of PAHs formed depends critically on the physical and chemical conditions, the relative concentrations of these stable PAHs do not. This table is mainly concerned with the pericondensed PAHs which are thermodynamically favored (105). The abundance of hydrocarbons with the same number of carbon atoms but a larger hydrogen content and a less stable structure is much lower (98). For example, the abundance of the 5 ring, benzo[g,h,i]fluoroanthene and cyclopenta[c,d]pyrene is two orders of magnitude larger than that of triphenylene, chrysene, and benzoanthracene. Likewise, apart from coronene ($C_{24}H_{12}$), no isomers of this fully condensed benzonoid have been detected in sooting flames. Finally, the high abundance of species containing pentagons (eg., acenaphthalene) is not surprising in light of the discussion above. Searches for these PAHs in the outflow from C-rich giants will be very valuable to test the similarity of dust formation around C-rich giants with that of sooting flames, to elucidate the actual carbon condensation pathway and to determine the relative importance of different interstellar PAH species. Of course, the distribution of PAHs ejected by these objects will be further modified by processes in the diffuse interstellar medium. In particular, UV photodissociation and photoisomerization will play an important role in weeding out less stable as well as small PAHs in the diffuse interstellar medium (107).

The formation of carbon stardust in the outflow from carbon-rich red giants is, thus, expected to be alike to the formation of soot in flames. Numerous laboratory experiments suggest that PAHs are, if not an essential intermediate, at least an abundant side product of the soot formation process. The infrared spectra observed towards many planetary nebulae (the red giants "daughter") show emission features at 3.3, 6.2, 7.7, 11.3 μm as well as broad underlying emission component (7). Although the observed spectra compare very well to that of carbon soot particles, energetic considerations imply that the species emiting the emission features are very small (20-50 carbon atoms; 10,11). They are, thus, a collection of free-flying molecules rather than clustered in soot particles. The broader emission components as well as the far infrared continuum is evidence for the presence of larger PAHs and soot particles (58, 108). Finally, we note that the ratio of C in PAHs relative to that in soot observed in planetary nebulae (≈20; 108) is in reasonable agreement with that measured for sooting flames (cf., table 5).

D) Non-LTE and the formation of C stardust

The conditions in the outflow from carbon-rich objects are probably far from being in thermodynamic equilibrium and this should have a profound influence on the carbon dust condensation process. For example, the vibrational excitation temperature of molecules in the dust condensation zone may be higher than the kinetic gas temperature due to radiative excitation by stellar photons or the trapping of line radiation (109). Since reaction rate constants are often very sensitive to vibrational excitation, some reactions may proceed much faster than expected from the kinetic gas temperature. The chemical composition may also be far from equillbrium. This is in particular true for the expected H/H_2 ratio. In the photosphere H_2 is formed by three body reactions and the H/H_2 ratio freezes out when the density drops below about 10^{11} cm^{-3} (110). This results in a disproportionally large abundance of atomic H farther out in the flow. The atomic H abundance is also influenced by the strong shock waves in the extended photosphere. Shock velocities can be as high as 25 km s^{-1} and H_2 dissociation will be important. Since the post shock density may be less than the freeze-out density, large deviations from the expected H/H_2 ratio may occur.

Finally, ionization may play an important role. Although no ionizing radiation is expected from a cool red giant, chromospheric radiation may play a (ionizing) role in supergiants. Moreover, chemiionization has been shown to be an important ionizing process in sooting flames. Of particular importance are the reactions

$$O + CH \rightarrow HCO^+ + e^-$$

$$CH(A^2\Delta \text{ or } B^2\Sigma) + C_2H_2 \rightarrow C_3H_3^+ + e^-$$

These ions are present in the reaction zone in sooting flames and their abundance falls off in the burnt gasses. Reactions between these ions and neutral molecules are rapid, as is isomerization into their most stable form (eg., PAH ions for the larger ones). They may actually play an important role in the soot nucleation and condensation process (90, 111). As for the neutral PAHs, pericondensed structures, such as $C_{13}H_9^+$, $C_{17}H_{11}^+$ and $C_{19}H_{11}^+$, are thermodynamically favored and observed to be most abundant in flames. In the circumstellar case, however, oxidation occurs in the stellar photosphere and little atomic oxygen (or CH) is expected to be present in the outflow. Cosmic rays which have sometimes been considered as an ionizing agent

are unlikely to play a role, since they are tied to the galactic field (gyro radius ≈ 10^{13} cm), which will be wrapped around the bubble blown by the stellar wind. Thus, ionization processes may be much less important in circumstellar shells around carbon-rich giants than in sooting flames.

E) Carbon stardust formation around WC 8-10 and R Cr B stars

The formation of carbon dust around R Cr B stars and WC 8-10 stars is expected to follow a completely different chemical pathway than in the outflow from C-rich giants. These objects have lost most of their H-rich envelope either through nuclear burning or through previous mass-loss. The reaction scheme derived above from experimental studies of the pyrolysis of hydrocarbons in sooting flames (cf., figure 8), which may be very relevant in the outflow from C-rich red giants, will play no role in the carbon dust formation in these objects, since no C_2H_2, C_2H or H is present. Carbon soot formation is now expected to be initiated through the formation of polyynes (eg., acetylene-like C chains withouth H; ie., C_2, C_3, C_4, etc). Large molecular structures of this kind (>20 carbon atoms) are expected to be flexible enough to form an aromatic ring structure. One important difference between this soot formation scheme and that involving acetylene and PAHs discussed above is the presence of a large number of unfilled valences at the periphery of the planar aromatic structure. Therefore, even more than in pyrolysis of hydrocarbons where H can (temporarily) saturate these dangling bonds, minimizing this "surface free energy" is expected to be very important in soot formation in R Cr B and WC 8-10 stars. This may act to enhance the value of pentagons in the aromatic structure (eg., minimize the number of surface bonds). The introduction of pentagons induces warping and curling of the aromatic planes, which may lead to closure of the aromatic structure on itself, again minimizing the number of dangling bonds. Indeed, laser vaporization studies of graphitic materials under a H poor atmosphere clearly illustrate the importance of such considerations (96,97).

A second difference between the outflow from these objects and that from C-rich giants is the presence of ionizing radiation. WC 8-10 stars are very hot stars and most of their energy is emitted in the far ultraviolet. Indeed, the wind from these stars is highly ionized. The observed column density of neutral C is typically only 10^{-6} of the elemental C. R Cr B stars are much cooler (cf., table 3), but they do possess an active chromosphere, emitting FUV radiation which may lead to ionization (as well as photodissociation). In this case simple, neutral, carbon bearing molecules do, however, dominate the composition of the envelope. Because ion-molecule reactions are much faster than neutral-radical reactions, ionization may play an important role in soot formation, in particular in WC 8-10 stars. The bottleneck in soot formation is now the formation of the first molecules. In view of the high degree of ionization, the absence of H, and the low pressure, radiative association of C with C^+ and C_2^+ are expected to be important reactions in the outflows from WC 8-10 stars. Dissociative recombination of C_3^+ will lead to C_2 which can then be used as a buildingblock towards larger acetylenic and aromatic species through ion-molecule reactions. Because of its low formation temperature, the carbon dust is expected to be highly disordered. Indeed, the IR spectrum of Ve 2-45 shows a weak emission feature at about 7.7 μm, which is attributed to the C-C stretch of aromatic carbon (112). This feature is only expected in disordered carbon with an aromatic domain size less than about 50Å (1).

F) Carbon stardust formation in supernova ejecta

It is appropriate to consider briefly the formation of carbon dust in supernova ejecta both because of the (possible) contribution of supernovae to the carbon budget of the galaxy (cf., table 2) and the presence of a carbonaceous component in meteorites containing isotopic anomalies characteristic of supernovae (3,113). Although IR excess emission has been detected in several supernova remnants, this may actually result from preexisting dust which "lights" up due to the SN (eg., infrared echo) and there is presently no conclusive evidence for the formation of (carbon) stardust in SN ejecta (47). Because of its timely nature, this discussion will be mainly geared to the recent supernova in the Large Magelanic Clouds (SN 1987a).

Supernova 1987a in the LMC is thought to result from the explosion ($\approx 10^{51}$ erg) of a slightly metal-poor star with an approximately 6 $M_\odot$ He core and a 5-10 $M_\odot$ H envelope (114,115). The main-sequence progenitor, SK-202-69, probably had a mass of about 20 $M_\odot$ and had undergone considerable mass-loss, presumably in a preceeding red supergiant phase, as evidenced for example by the detection of a nitrogen-rich circumstellar shell (116). For our purposes we only need to consider the He core in which static He burning has produced a large mass fraction of ^{12}C. Explosive nucleosynthesis following the passage of the shock front will convert a large fraction of this core into heavier elements, but a carbon-rich zone containing about 2 $M_\odot$ remains (115). The competition between different heat sources (diffusion of radioactive heat due to decay of freshly synthesized ^{56}Co; H recombination; possible pulsar) and sinks (adiabatic expansion; radiation) hampers an acurate prediction of the temperature-pressure history of the He core material. Uncertainties in the opacity due to velocity shearing, compositional gradients, as well as mixing of different zones due to Rayleigh-Taylor instabilities further compound this problem (115). Indeed, estimates of the gas pressure in supernova ejecta, when the kinetic temperature reaches the typical dust condensation temperature of about 1000K, vary by about 10 orders of magnitude (117). As a result of these uncertainties, predictions of grain formation in SN 1987a resemble a weather forecast: it may rain grains or it may not.

G) Summary

This detailed examination of the chemical pathway towards soot has identified several important physical concepts and, although there is some "loose" correspondence, the distinct differences between the kinetical and thermodynamical approach should be stressed. Clearly, the role of hydrogen in soot condensation cannot be overemphasized. Hydrogen saturates the free valences at the periphery of the aromatic nucleation centers and thereby reduces its surface free energy. As a result surface free energy plays much less a role in dust formation than envisioned by classical nucleation theory. That C_2H_2 rather than C is the gaseous precursor molecule to soot is a further distinction between the chemical and classical approach. The saturation with H implies that kinetic effects are very important, since a peripheral H has to be abstracted before further chemical growth can occur. Such kinetically controlled growth will lead to a highly disordered structure of the resulting condensates. The dominant role of H in soot formation is exemplified by the high abundance of PAHs as well as the high H content of soot. Physical growth (ie., clustering) can also play an important role in determining the final size and gross structure of the product (cf., fig. 7). At what point clustering of microcrystals overtakes chemical growth by monomer addition will depends on the detailed temperature and density history of the cooling gas. Finally, this discussion pertains

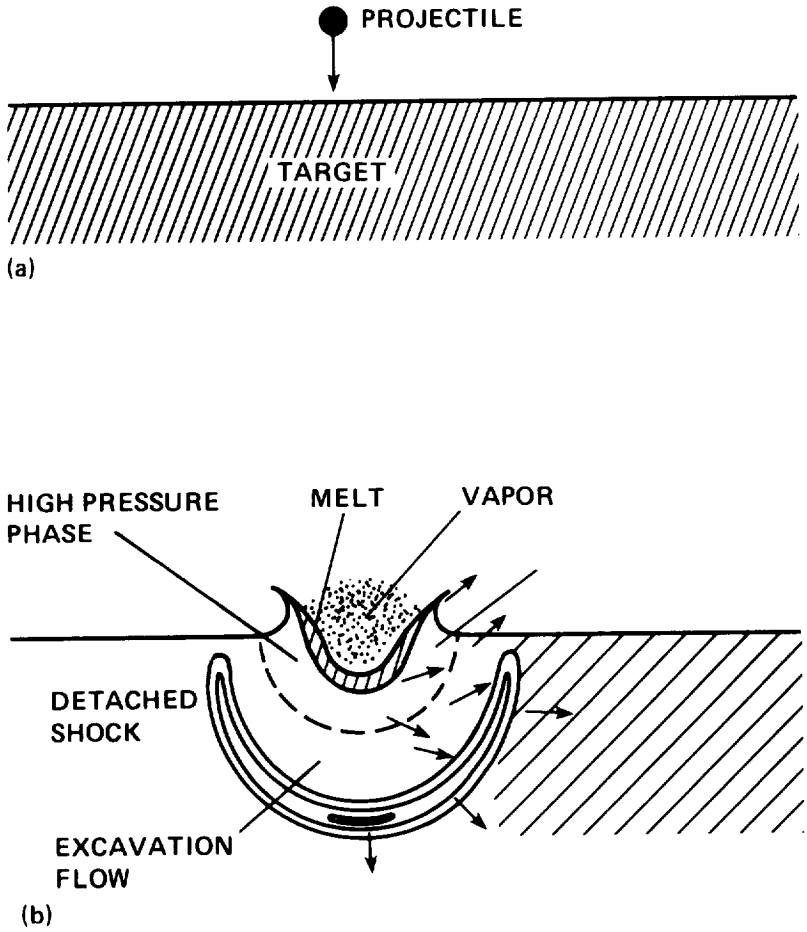

Figure 10. A schematic representation of the impact of a projectile on a target. The fate of the shocked target material depends strongly on the peak shock pressure. Since the strength of the shock wave driven into the target decays with distance, the impact point is surrounded by successive zones in which the target has been vaporized, molten, or converted into a high pressure phase (eg., diamonds). The arrows indicate the velocity vectors in the excavation flow which will carve out the final crater (see text for details).

to soot formation in a hydrogen-rich atmosphere. When H is absent, as in WC 8-10 stars, the chemical pathway towards dust will be quite different, leading perhaps to a different soot structure. Ions or Buckminsterfullerene rather than PAHs may be the reactive intermediaries. Nevertheless, it is expected that kinetic rather then thermodynamic effects will control soot formation and the structure of the resulting grains.

VII Grains and Shocks in the Interstellar Medium

Strong shock waves generated by supernova explosions are the dominant destruction mechanism for interstellar dust grains (118-121). Behind the shock front, the charged grains gyrate at high velocities around the magnetic field lines. Impinging gas atoms can sputter atoms from the grain surface (non-thermal sputtering), while collisions with other grains can lead to partial and complete vaporization. Evidence for destruction of interstellar grains by shock waves is provided by the observation that high velocity ($v \approx 100$ km/sec) interstellar gas (presumably recently shocked) has much higher elemental abundances in the gas phase than the general interstellar medium (122,123). Although grain destruction by sputtering and vaporization have received the greatest attention in the literature, shattering and phase transformations due to grain-grain collisions are equally important. The study of phase transformations due to grain-grain collisions in interstellar shocks has recently gotten additional impetus by the discovery of small (≈50Å) diamond grains in carbonaceous meteorites (124). This carbon phase (socalled C-δ), which comprises about 2% of the elemental carbon, contains isotopic anomalies which presumably originated outside the solar system (3). These meteoritic diamond grains may result from shock processing of interstellar graphite or amorphous carbon grains. High velocity (>8 km s^{-1}) grain-grain collisions behind strong supernova shock fronts are expected to produce the high pressures required to transform these carbonaceous materials into diamond. Such collisions are predicted to produce polycrystalline diamonds with microcrystal sizes ranging from about 5 to 100Å, possibly intermixed with some highly disordered diamond (125).

Behind the shockfront small grains (<500Å) are rapidly dragged to a halt through collisions with the gas. Essentially, because of their larger volume to surface ratio, large grains will not be stopped as quickly (cf., 121). Extinction observations show that interstellar grains have a steep size distribution ranging from about 3000Å to molecular sizes (13-17). Most of the interstellar grain volume is in the large grains, but the surface area is in the small ones. The most important grain-grain collisions behind a shock are thus due to a large grain impacting a small grain at high velocity.

A) Grain-Grain collisions

Initially, when a projectile impacts a target at high velocity, strong planar shock waves are driven into both target and projectile at nearly constant pressure and velocity as the kinetic energy of the collision is thermalized. This first stage ends when the shock wave in the projectile has reached the back surface and is reflected as a rarefaction wave which eventually reaches the target. These rarefaction waves as well as the expansion of the shock wave from the impact site will transform the planar shock in the target into a more or less hemispherical form (eg., the detached shock; see figure 10) and its strength will decrease with distance from the impact

site. In this second stage the shock pressure will drop approximately inversely with the engulfed volume ($P \sim V^{-1.1}$) where the small deviations from the solution for a Sedov-Taylor blast wave are due to the backsplash of ejected material which carries away energy and imparts momentum (126,127). The rarefaction waves from the free surfaces will set up a flow pattern for the shocked material upward and away from the impact site (eg., the excavation flow; see figure 10). During the excavation of the crater, some of this material reaches the free surface and can be ejected as small, shattered fragments. The remainder will line the crater. Shattering may also occur when the shock breaks through the backside of the target and is reflected backwards as a tensile wave (ie., spalling).

The rarefaction wave that follows the shock wave will release the compressed material and during this expansion the shocked material may undergo a phase transformation. For very strong shocks, the pressure is high enough to cause vaporization. For weaker shocks, the material can unload into the liquid phase, or into a high density solid phase such as diamond. A shock slows and weakens as it expands through a target, so that an initially very strong shock successively vaporizes, melts, transforms and shatters the target (cf., figure 10). Clearly, the process with the smallest threshold pressure will affect the largest volume. Assuming the experimentally measured threshold pressure for the graphite-diamond transition of 600 kbar (i.e., threshold energy ϵ=0.7eV/C atom; cf., § B) and for vaporization of 5.7 Mbar (i.e., a binding energy ϵ=7.5eV/C atom), the ratio of the volume of diamonds produced relative to that vaporized is about 7.5 for semi-infinite targets. Of course, for high velocity impacts of equal-sized grains both grains will be vaporized, but those collisions are fairly rare. Nevertheless, for interstellar grain-grain collisions a careful analysis has to be carried out taking into account the expansion of the shock wave in the target as well as the finite-size of the grains. The threshold collision velocity for diamond formation is the sum of the particle velocity behind the shock in the target and projectile ($=2(2\epsilon/m_c)^{1/2}$; m_c=mass of C atom), corresponding to 6.8 km s^{-1}. Likewise, the threshold collision velocity for vaporization is calculated to be about 23 km s^{-1} assuming a threshold energy equal to the binding energy. Actually, because of kinetic effects, the shock will have to supply several times the binding energy to cause appreciable vaporization (127,128) and this estimate as well as that of the relative volumes is only a lower limit.

In order to estimate the effects of grain-grain collisions in interstellar shock waves on interstellar grains several different steps have to be taken. First, for a given size ratio of projectile and target grain the diamondized volume (or vaporized/shattered) is calculated as a function of relative grain-grain collision velocity, taking the finite size of target (and projectile) into account. This volume is averaged over impact parameter, since glancing collisions couple less of the projectile's energy and momentum to the shock wave in the target (127). This is then used as input for a numerical code which calculates the structure of an interstellar supernova shock wave (120,129). Behind a supernova shock front different sized grains have a different velocity history and thus for each grain size at each spatial point in the postshock gas the collision rate with all other grains has to be weighted with the grain volume affected by such a collision. Integration over position behind the shock yields then the diamondized volume for each grain size. The total grain volume that is diamondized by a supernova shock at one particular shock velocity is then calculated by integrating over grain size. This calculation is repeated for several different supernova shock velocities. Finally, these volumes are convolved with the frequency a

grain is shocked by a supernova shock with a particular velocity to calculate the lifetime of a grain versus diamondization (or vaporization or shattering). This latter step requires a model for the interstellar medium. Evaluation of these integrals yields an expected fraction of elemental carbon in small diamond grains of about 5% (127). This fraction is not very dependent on the absolute supernova shock frequency since supernova shocks both form and destroy (through sputtering and vaporization) diamond grains. Of course, the large number of other steps required in the evaluation do make this number quite uncertain. Nevertheless, since observations of elemental depletions in high velocity gas testify to the destruction of interstellar grains by supernova shock waves, a small fraction of the elemental C (≈5%) is expected to be in the form of interstellar diamonds produced by grain-grain collisions in the interstellar medium.

B) Diamond metamorphism

Numerous laboratory experiments have shown that graphite and amorphous carbon transform into polycrystalline diamond (crystallite size≈200Å) by a diffusionless process when a shock wave traversing these solids drives the pressure above about 400 kbar. The transformation is complete when the pressure exceeds about 600 kbar (130-135). Experiments have been performed on fairly well ordered forms of pyrolytic graphite (i.e., polycrystalline carbon), on slightly disordered, natural graphite from Ceylon, as well as on highly disordered and porous forms of graphite. For the more disordered forms the threshold pressure for complete diamond transformation is actually somewhat lower (≈400kbar). Because of the high activation energy (≈7.5eV/C atom) for the diamond-graphite rearrangement, graphitization of newly formed diamond will not occur when the cooling behind the shock front is very rapid. Indeed, experiments have shown a high conversion efficiency. Even at shock pressures of only 250kbar, well below the complete transformation threshold, about 25% of diamonds have been recovered (135). A single, perfect crystal of graphite, when shocked along the c-axis, actually transforms into a hexagonal form of diamond (i.e., lonsdaleite) rather than the cubic form.

The carbon phase diagram: Figure 11 shows the high pressure phase diagram for carbon (136). Three different regimes can be discerned, where graphite, diamond and the liquid phase respectively are thermodynamically stable. The liquid-diamond transition has been shown with a positive slope, reflecting recent theoretical and experimental studies (137,138). Although diamond is thermodynamically favored at high pressures and temperatures, graphite is metastable in part of this regime, presumably because the transformation entails a complete rearrangement of the carbon lattice. Likewise, diamond is metastable in part of the graphite domain. Measurements of the metastable graphite melting curve within the diamond stability regime (eg., between about 2500 and 4000 K; 136) have been boldly linearly extrapolated to much lower temperatures in figure 11. Theoretical calculations show that a metallic carbon phase with a simple cubic structure is preferred at very high pressures (>10Mbar; 139). Although preferred at high temperatures and low pressures, the exact location of the vapor phase is not well known. Estimates of the solid-liquid-vapor triple point range from about 0.1 kbar and 4500K to about 2×10^{-4} kbar and 4000K (136). Essentially this uncertainty reflects a debate on the existence of a fourth polymorph of carbon which may have been detected in some carbonaceous meteorites and in chaotite from the Ries impact crater (140,141). In this solid, known as carbyne, the carbon is thought to be arranged in linear chains either with alternating triple and single bonds (acetylene polymer; cf., figure 2) or with

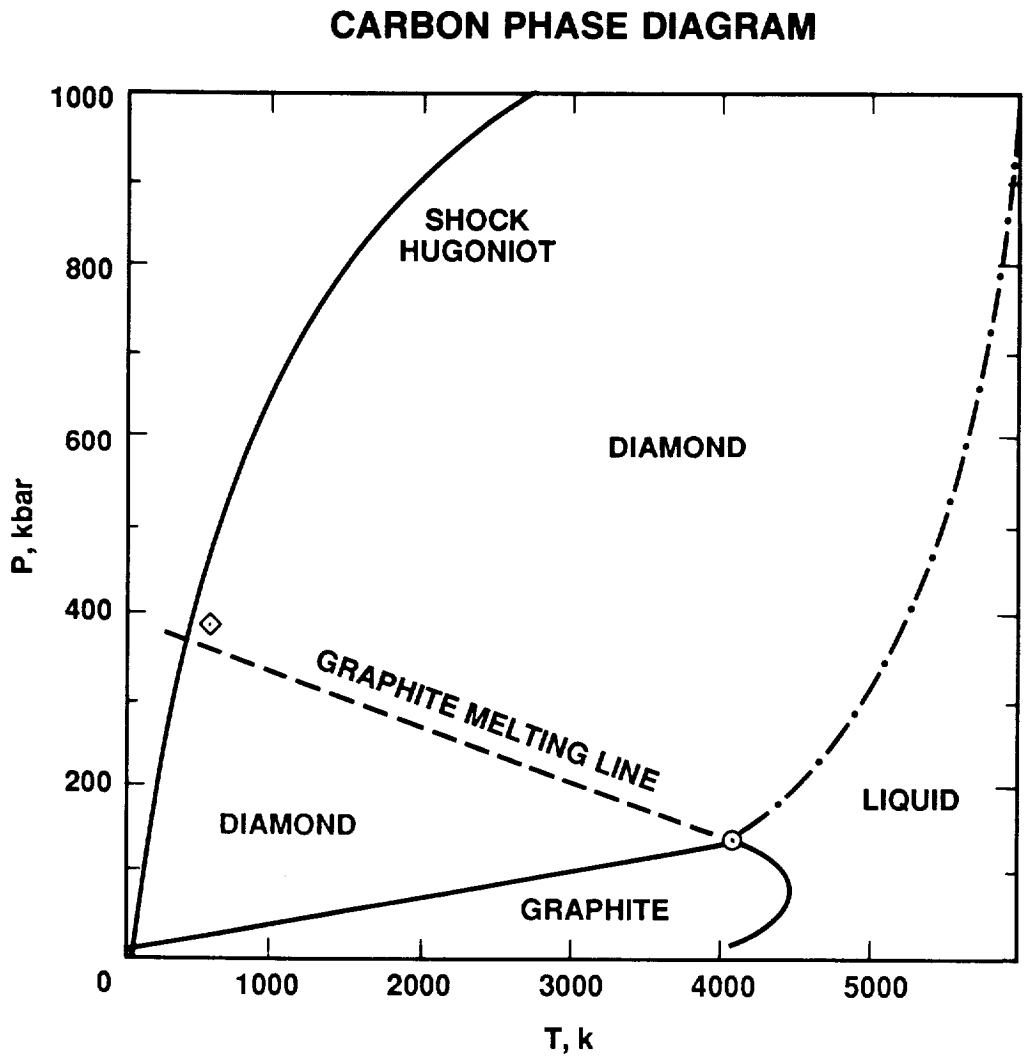

Figure 11. The carbon phase diagram at high pressures and temperatures (adapted from reference 136). The regimes in which graphite, diamond and liquid carbon are thermodynamically favored are indicated. Graphite is metastable below the graphite melting line within the diamond stability regime. Diamond is metastable below about 2000 K in the graphite stability field. The line labeled shock Hugoniot connects the loci of shock states accessible for graphite. The stronger the shock the further to the right the immediate post shock conditions will be. The diamond symbol indicates the experimentally determined threshold conditions required for the graphite -> diamond transformation.

cumulated double bonds (cumulene; 142). However, although carbon in the form of acetylene polymers could certainly be metastable in a large part of the phase diagram, the existence of this fourth stable carbon polymorph has never been shown directly. Moreover, the original discovery is very much in doubt, since later research on several of these samples either discovered impurity inclusions in these materials or could not repeat the earlier results (143).

The graphite shock Hugoniot (144) has been superimposed on the carbon phase diagram (cf., figure 11). The Hugoniot is the loci of shock states accessible for graphite. The higher the shock velocity, the higher the resulting postshock temperature and pressure will be and the farther to the right on the Hugoniot curve the material immediately behind the shockfront will find itself. After the passage of the shockfront the compressed material will expand again. This expansion is adiabatic and no entropy change will occur. For low postshock pressures, the expansion isotrope will almost coincide with the shock Hugoniot. For the high shock pressures appropriate for this discussion, the material can still contain appreciable internal energy after expansion and the expansion isotrope lies to the right of the Hugoniot. The approximate location of the shock conditions for which the graphite-diamond transition is first observed is indicated by a diamond in figure 11. Commercial production of (shocked) diamonds occurs typically up to about 1Mbar and 3000K (136,145).

The onset of the shock generated, graphite-diamond transformation occurs close to the extrapolated graphite melting line in the carbon phase diagram and is probably initiated by pseudo-melting of graphite and rapid recrystallization in the diamond phase (136,146). Extrapolation of these laboratory studies to interstellar grain collisions is somewhat hampered by the difference in scale size. Laboratory determined crystallization timescales are faster than 10^{-8} s (135), but this may still be longer than the adiabatic shock cooling timescale in an interstellar grain ($\Delta r/C_s \approx 10^{-12}$ s, where Δr ($\approx$100Å) and C_s ($\approx$5 km s^{-1}) are the size and sound velocity in the compressed material) and the resulting crystal may be highly disordered. Note that although the shocked region may be optically thin at the small interstellar grain size scales, radiative losses due to electronic or vibrational transitions are not important since the radiative lifetimes (for aromatic molecules $\approx 10^{-8}$ and 0.1 s, respectively; 147) are much longer than the adiabatic expansion timescale.

Microcrystal sizes: Near the melting line the structure of monatomic liquids is that obtained by dense random packing of hard spheres (148,149). Energy and strain considerations favor then a local liquid structure consisting of 20 tetrahedra arranged in clusters of icosahedral symmetry (containing 13 carbon atoms; 150,151). These abundant icosahedral clusters can act as nucleation centers for crystallization into an ordered crystal structure. The rate at which atoms in the liquid-solid interface move to lattice sites is limited by the sound velocity (eg., vibrational timescale, $\approx 10^{-14}$ s). The advancing liquid-solid interface will be driven by the liberated latent heat of melting at velocities up to the sound velocity (explosive crystrallization; 152). That is,

$$v_l = K \frac{dT}{dr} / \Delta H_m$$

where K is the heat conductivity ($\approx$3 W cm^{-1} K^{-1} for diamond at 1000K; 153) and dT/dr is the temperature gradient ($\approx 10^9$ K cm^{-1} for a 100Å compressed region). The latent heat of melting of diamond, ΔH_m, is not known. Assuming it is the same as for graphite ($\approx$25 kcal/mol; 136) yields $v_i \approx 1$ km s^{-1}. Crystallization will stop when neighboring diamond crystals touch or when the heat loss to the surroundings becomes too large. The remainder of the carbon liquid will then cool so rapidly that it will solidify in a highly disordered diamond structure (c.f., 1). Probably, this will become important when the compressed material has expanded again due to the rarefaction wave. The diameter of the (ordered) diamond crystals grown this way will then be set by the crystal-liquid interface velocity, v_i, and the time available, (ie., $\Delta a \approx 2v_i/C_s \Delta r$). This limits the size of a diamond microcrystal to the size of the expansion region behind the shock (Δr), which is typically about 10% of the depth of the shock front in the target (154). For the formation of interstellar diamonds, collisions of small (100Å) grains with large carbon ($a \approx 1000$Å) grains are most important resulting in a Δr of 100Å. For the parameters quoted above we find that Δa is typically 40Å. Note that this is to first order independent of the size of the expansion region, essentially because the crystal-liquid interface velocity adjusts itself to the size of the expansion region. It is therefore not very surprising that the sizescale of the microcrystallites in macroscopic experiments ($\approx$100Å; 135,145,155) is very similar to those expected in the collision of submicron particles.

Once the liquid has solidified, further rearrangement of the lattice will be inhibited by a considerable activation barrier. Therefore, the bonds between carbon atoms in the interfaces of neighboring microcrystals will be higly strained and distorted. As a result these interfacial carbon atoms will show some degree of sp^2 bonding (cf., fig. 2). This will give an apparent "amorphous carbon" character to some types of spectra (cf., 124,156). Both laboratory produced diamonds as well as meteoritic diamond reveal the presence of such highly disordered interfacial carbon (156). Upon cooling and expansion, the shock synthesized diamond will enter the graphite stability regime. Graphitization of the newly formed diamonds will, however, be inhibited by a large energy barrier since all the bonds have to be broken and the lattice rearranged. Diamond is therefore metastable below 2000K in the graphite stability field. Since a large fraction of the carbon is recovered as diamonds in macroscopic shock experiments of graphite and since cooling will be even faster, graphitization is expected to be unimportant on the submicron sizescale of interstellar grains. We note, however, that ion-implantation during further shock processing will lead to an approximately 5Å thick, amorphous, surface layer in which the binding has an aromatic character (127).

Finally, in those cases where spalling is important (see below), a small fraction of the compressed material may be released during the spalling process. In that case, the sizes of the resulting fragments will be determined by the surface free energy of the high pressure carbon liquid and the resulting solidified droplets may be somewhat smaller.

Shattering: For the prediction of the structure of interstellar diamonds the effects of shattering must also be considered. The velocity associated with the excavation flow which carves out the crater in the target is much less than the velocity of the rarefaction wave and thus the molten material is expected to solidify long before

shattering at the free surface can occur. It is important to recognize that the fracture yield strength is highly size dependent (127,157,158). For macroscopic bodies shattering is due to the initiation, growth and coalescence of microscopic cracks, but these play no role at micron size scales where materials will show a ductile (fluid) rather than brittle behaviour. The dynamic yield strength of polycrystalline diamond is measured to be about 400 kbar (159,160). This is very similar to the minimum dynamic pressures required to form diamond by shock-metamorphism. Since the pressures associated with the excavation flow are much less than those of the shock and since most of the shock diamond synthesis occurs at the lowest pressures ($V \sim P^{-0.9}$; cf., § VIIB), shattering during crater formation is expected to be of little importance. Shattering can also occur when the shock reaches the backside of the target and is reflected as a tensile wave (eg., spalling). However, in view of the increased tensile strength of materials at small sizescales, this plays much less a role than for macroscopic bodies. Indeed while "catastrophic destruction" of cm-sized glass spheres occurs for pressures of the order of one kbar (161-163), for submicron-sized glass spheres the critical pressure is of the order of 150 kbar (127). For shock synthesized diamonds this critical pressure is expected to be around 400 kbar. Assuming that the typical diamond forming collision occurs between a 100Å and a 1000Å grain, the minimum collision velocity for catastrophic destruction is then calculated to be about 100 km s^{-1} (127). Since diamond formation in the interstellar medium is dominated by low velocity shocks ($V \approx 50$ km s^{-1}; 125), shattering of newly formed diamonds is expected to be relatively unimportant.

Impurities: Interstellar graphite or amorphous carbon grains may contain considerable amounts of impurities, either interstitial or substitutional. In particular, stardust formed in the outflows from carbon-rich red giants may be heavily hydrogenated ($H/C \approx 0.1$; cf., § VIB). Some impurities, such as N, can be substituted for C in the diamond lattice and their presence will not have a major effect. Hydrogen (or deuterium) atoms are small enough that they can be stored in interstitial diamond sites. Natural diamonds contain typically about 0.3% of substitutional nitrogen, which in fact gives them their striking colours. About 0.2% of interstititial and often a similar amount of chemically bonded hydrogen is also present (164). Small amounts of impurities will not affect the shock Hugoniot or the graphite-diamond transformation very much. Indeed, diamonds have been recovered from shock experiments on glassy carbon (highly disordered C resulting from heat treatment of furfural resins) containing up to 10% of oxygen, 3% of hydrogen and 0.2% of nitrogen (165). In principle, larger amounts of impurities might lead to different results. Nevertheless, theoretical and experimental studies of liquid benzene shocked to about 700 kbar indicate that some of the carbon is transformed into diamond, although no recovery studies have been performed (166). However, we do note that small diamonds have been recovered in static pressure/flash heating experiments on several organic compounds, including anthracene, naphthalene, chrysene and pyrene (167). The threshold conditions for diamond formation in these experiments seems to be somewhat higher than for pure graphite experiments (168). Thus, it is likely that even a fraction of "impure" amorphous carbon grains such as hydrogenated amorphous carbon formed around carbon-rich red giants will transform into diamonds under shock conditions.

In the context of the small diamonds discovered in carbonaceous meteorites, the fate of interstititial impurities such as Xe HL is of considerable interest. Pulsed laser

annealing studies of ion-implanted silicon layers show for example that, due to diffusion during the liquid phase, impurities are concentrated near the surface of the crystals (169). The measured crystal-liquid interface front velocity in these experiments is about 1 m s^{-1}, which is less than the effective "diffusion" velocity ($\approx$10 m s^{-1}; 169). However, crystallization will occur much faster than diffusion in the interstellar case and (inert) impurities are expected to be incorporated into (and distort) the diamond structure.

C) Diamonds in the sky

Since only a small fraction of the elemental C is expected to be in the form of diamond grains due to shock processing, it may be difficult to detect them in the interstellar medium. Small diamond grains will show a pronounced far ultraviolet absorption edge and may contribute to the far ultraviolet rise in the observed interstellar extinction curve (125). However, a size distribution of large (polycrystalline) diamond grains will produce a rather smooth extinction curve over the visible and UV (170). In that case, the presence of diamond grains will be difficult to prove (or negate), since the extinction will be dominated by other more abundant dust components (cf., table 1). The density of phonon states of diamond shows several peaks between 4.5 and 5μm, but these modes are IR inactive for a perfect monovalent crystal and thus for large, crystalline diamonds. However, some IR activity is induced by the disorder introduced by the presence of impurities, defects and particularly microcrystallite surfaces (1). Thus, higly disordered, interstellar, diamond grains, resulting from rapid quenching of the liquid (cf., § B), will show weak infrared signatures at the peaks of the phonon density of states.

The interlocking microcrystals in the polycrystalline diamond grains will be separated by highly disordered thin interface regions. The carbon atoms in these regions have a large sp^2 character (eg., aromatic structure; cf., fig. 2) and their IR spectrum will resemble that of soot. These polycrystalline conglomerates might contribute to the widespread, near-infrared (12μm) cirrus observed by IRAS (125). Note that, in contrast to small PAH molecules, they absorb over a large part of the visible and UV region of the spectrum without showing distinct structure in the extinction curve. Moreover, their IR emission spectrum will be very similar to that of soot and is therefore likely to resemble that observed in reflection nebulae (8). Third, because most modes are IR inactive, these grains will radiate more easily in the mid IR than other materials with comparable sizes. A high temperature is also indicated by the high Debye temperature of diamonds. Moreover, due to the difference in structure and binding, it is perhaps possible to localize the excitation energy in a small (amorphous carbon) part of the polycrystalline grain, which will temporarily be excited enough to radiate through the near- and mid-infrared modes (171). Obviousy, laboratory studies will be very important to study the reality of such energy localization effects.

VIII Interstellar Carbon Dust and Carbonaceous Meteorites

One of the most interesting developments within the field of interstellar dust in recent years is the realization that some interstellar grains may have been incorporated into meteorites and interplanetary dust particles without totally losing their identity (3,113,172). Evidence for this rests on the measurement of isotopic

anomalies in meteorites and in particular in carbonaceous chrondites. Although the meteoritic composition is in a global sense remarkably homogeneous, non-mass-dependent isotopic anomalies do exist for many elements. These include the noble gases, the light elements (H,C,N, and O), and the heavy elements (e.g., Ca, Ti, Cr, Ni, Nd, Sm and others). Although some unusual processes in the solar nebula might have produced non-mass-dependent isotopic fractionation in some elements, it is unlikely that they could account for all of them. Moreover, the measured isotopic anomalies are very characteristic for a presolar origin of the material. For example, the Xe and Kr isotopic anomalies associated with one particular meteoritic carbon phase carry the signature of s processes in red giants, suggesting the presence of largely unmodified carbonaceous grains in meteorites which were produced in carbon-rich red giant outflows (17,25). Thus, meteoritic materials carry a nucleogenic record of the birth site of the dust grain, modified by processes which occured in the interstellar medium as well as in the solar nebula or on planetary bodies. Consequently, laboratory analysis of meteoritic and interplanetary material may yield detailed microscopic information on interstellar dust, which is not obtainable by astrophysical observations. It should, however, be emphasized that meteoritic materials are very heterogeneous and contain dust grains from different origins; including star dust from many different birth sites, interstellar medium dust, and solar nebula condensates. Generally, the actual presolar carrier of the measured isotopic anomalies is not known. Such information is, however, of prime importance for our reading of this record and for our assement of the implications for interstellar dust and its evolution.

Many different carbon phases with isotopically anomalous composition have been discovered in carbonaceous meteorites. Table 6 provides a summary of some relevant data on these phases (cf., 113). Each of these will be discussed in turn.

The C-α phase: This phase consists of turbostratic carbon, that is a carbon solid containing disoriented graphitic layers quite similar to soot. It contains almost pure ^{22}Ne. Most of the ^{22}Ne in the galaxy is produced by WC stars. These stars also produce minor amounts of carbon stardust (cf., table 2) and thus might be the origin of this carbon phase in carbonaceous meteorites (173). However, it is difficult to produce almost pure ^{22}Ne this way. In particular, theoretical calculations of the nucleosynthesis in WC stars predict that the $^{20}Ne/^{22}Ne$ ratio is about 0.02 (44). An alternative source of ^{22}Ne is β-decay of ^{22}Na and novae are then an attractive source for this carbon phase (174). The freshly synthesized ^{22}Na, other Na isotopes (ie., ^{23}Na), as well as other elements (^{25}Mg, ^{26}Mg, ^{26}Al, ^{27}Al) must have been rapidly incorporated into the carbon stardust before the ^{22}Na decayed ($\tau \approx 2.5$ yrs) to ^{22}Ne. We note that electron donors such as alkali, alkaline earth and transition metals, readily form intercalation compounds with graphitic and turbostratic carbon (175). Unlike the noble gases these metals are, however, difficult to measure in meteorites.

This meteoritic carbon phase component is also known to be enriched in ^{13}C and ^{15}N (cf., table 6). However, the ^{13}C enrichment is less than one might expect from theoretical models for novae nucleosynthesis which predict $^{12}C/^{13}C$ ratios less than unity (30,53). Also ^{15}N overabundances of $>10^3$ are predicted by some models. These predictions are quite sensitive to the details in the models (temperature; mixing; shell burning) and the problem may reside in the nucleosynthesis models rather than the identification of this meteoritic carbon phase with novae stardust. Alternatively,

Table 6: Interrelationship of interstellar and solar system carbonaceous materials

Carbon Phase	Isotopic Anomaly	concentration [ppm]	Birth Site
C-α (Ne-E)	pure ^{22}Ne $^{12}C/^{13}C \approx 70$	5	-Novae
C-β	s process Xe $^{12}C/^{13}C \approx 40$ ^{86}Kr	<5	-C-rich Red Giants
C-δ (diamond)	Xe-HL $^{14}N/^{15}N > 400$ $^{12}C/^{13}C \approx 90$	400	-graphite -> diamond in ISM shock waves
C-ϵ	^{22}Ne $^{12}C/^{13}C < 10$	2	-Novae
soluble and dust	D/H up to 10^{-3}	20,000	-pyrolysis of ISM
insoluble organic matter	mundane C and N		-PAHs (?)

the C-α phase may be contaminated with solar system carbon with a normal $^{12}C/^{13}C$ ratio.

The C-β phase: This carbon phase in carbonaceous meteorites consists of SiC grains which contain enriched s-process isotopes of Xe and Kr (cf., table 6). It is also enriched in ^{13}C. It is generally accepted that this carbon phase represents stardust condensed out in the outflow from carbon-rich red giants (3,113,172), where we note that the 11.4μm feature, characteristic for SiC, is often seen in such environments (cf., table 1 and 2). The $^{14}N/^{15}N$ ratio in this carbon phase is solar, which is somewhat surprising since the same dredge-up episodes that enhance ^{13}C also will produce ^{14}N (176). Because of its refractory nature SiC is more readily detected in stepwise heating of carbonaceous meteorites than carbon dust. The latter is, however, more abundant in circumstellar and interstellar dust and a "pure" carbon phase with similar isotopic anomalies is expected to be present in carbonaceous meteorites at about the 50ppm level.

The C-δ phase: The C-δ phase in carbonaceous meteorites consists of small diamond (≈50Å) grains (124,156). Both the heavy and light isotopes of Xe are enriched compared to the sun, implying a presolar origin (3). It has been suggested that these isotopic anomalies reflect the effects of mixing of two different nucleosynthetic zones within one supernova. This may have occured either before condensation or

after condensation in one zone by ion implantation of the products of the second zone. A variant of the latter is ion-implantation in grains formed in a precursor mass-loss phase by the overtaking high velocity, supernova ejecta (177). Recently, it has been suggested that these small diamond grains are the result of shock metamorphism of carbon stardust in the interstellar medium (125). In that model, the measured isotopic anomalies reflect the sum of the nucleosynthetic processes taking place in the various birth sites of the original carbon stardust. Both the small ^{15}N and the absence of a ^{13}C enhancement are difficult to understand in terms of a single circumstellar source (eg., supernovae or their red supergiant progenitors) of this meteoritic carbon phase but might conceivably result from averaging over many different carbon stardust sources. In the latter case, one might however expect isotopic variations on an individual interstellar grain basis (≈1000Å scale). It should be emphasized that the measured abundances of the isotopically anomalous Xe are measured on μg samples and reflect thus an average over about 10^{11} diamond microcrystals or about 10^8 typical interstellar dust grains (≈1000Å).

The surface layers of this meteoritic carbon phase seem to contain noble gases impurities with an isotopically anomalous composition (113). These might result from ion-implantation. For a typical gas-grain drift velocity due to radiation pressure in WC 8-10 and supernova ejecta of 25 km s^{-1}, the ion range of Ar and Xe is 3 and 7Å, respectively. In this case, the implantation depth will, thus, depend to some extent on the mass of the element under consideration. Note that the drift velocity in red giant outflows is generally very small and ion implantation should be unimportant. Finally, appreciable drift velocities will also occur in interstellar shock waves and the resulting ion implantation will tend to dilute the nucleogenic record from the grain's birth site.

The C-ϵ phase: The C-ϵ phase consists of SiC grains carrying an almost pure ^{22}Ne enrichment. As was the case for the C-α phase, this phase is thought to represent stardust condensed in nova ejecta. An 11μm feature observed in nova Aquila has been attributed to SiC grains (48). Since the Si/C ratio in WC stars is expected to be very small, the identification of the carrier of this Ne E component with SiC provides an additional argument against an origin of the other Ne E component (the C-α phase) in WC stars, which have a very low Si abundance. The large enhancement of ^{13}C in these grains (cf., table 6) supports an origin in novae (30,53). It makes the much higher $^{12}C/^{13}C$ ratio in the C-α phase even more puzzling and suggests that the C-α phase is contaminated by solar system carbon with a normal $^{12}C/^{13}C$ ratio.

Organic matter: Two components are lumped together under this nomer (3,113,172). First, the acid-soluble fraction (≈25%) contains such organic compounds as amino and carboxylic acids. Second, the acid-insoluble fraction (≈75%) consisting of aromatic moities connected by short aliphatic bridges and sidechains (eg., kerogen). Both phases are heavily deuterated. Such chemical fractionation will only occur at very low temperatures (T<100K). Although the cooling solar nebula will have experienced such low temperatures, the timescale to reach this equilibrium is far too long to obtain a sizeable fractionation (3). High deuteration effects have been observed in many gas phase molecules in interstellar molecular clouds and are thought to originate from ion-molecule reactions (178). Large deuteration effects are also expected for icy grain mantles accreted in molecular clouds (179). These deuteration effects result from non-equilibrium chemistry driven by cosmic ray ionization and

equilibrium is readily established at interstellar timescales ($\approx 10^7$ yrs). For this reason the hypothesis that interstellar, as distinct from circumstellar material, has been incorporated into carbonaceous meteorites without major modifications has been widely accepted (3, 172,180). The actual deuterated carrier(s) into the solar nebula, whether gas phase or solid state, and the importance of the distinction between the soluble and insoluble phases is unknown. Possibly, the kerogen results from clustering of small interstellar PAH molecules and amorphous carbon grains, where the PAHs carried the deuteration effects due to photochemical processes in the interstellar medium (181). Alternatively, it may result from prolonged pyrolysis of (deuterated) interstellar molecules either in the solar nebula (3) or in the interstellar medium (2). In the latter model the acid-soluble phase may represent an intermediate step in the UV photolysis and transient heating of interstellar grain mantles. Indeed, laboratory studies show that carboxylic acids are readily formed from simple molecular ices (eg., H_2O and CO) by such processes (182,183). Prolonged exposure to UV radiation and transient heating is expected to result eventually in the almost complete removal of elements other than C (and possibly H) and to lead to a structure similar to that of meteoritic kerogen.

IX Summary

In summary, we conclude that interstellar dust is a collection of many different materials. There are many different stardust birth sites each with distinct physical and chemical conditions and elemental and isotopic composition. Many different types of objects contribute to the carbon budget of the galaxy, including WC stars, supernovae and carbon-rich red giants. Although the relative contribution of each of these is not well known, it is likely that both low mass and high mass stars contribute about equally. Astronomical evidence shows that carbonaceous stardust originates in WC 8-10 stars, C-rich red giants, and possibly supernovae. Studies of meteoritic carbon compounds strongly suggest that some novae produce SiC and amorphous carbon grains. Probably carbon-rich giants dominate the carbon stardust balance. About 20% of the elemental C is injected in the form of dust grains. Since extinction observations suggest that about half of the elemental C is locked up in dust grains, this implies the presence of an efficient formation mechanism for carbonaceous dust in the interstellar medium. One attractive mechanism is UV photolysis of accreted icy grain mantles, which may result in organic refractory grain mantles (polymeric carbon) or perhaps even amorphous carbon grain mantles.

The physical conditions in the stardust condensation zone around C-rich giants, R Cr B stars and WC stars have been reviewed. These objects span a wide range in physical and chemical conditions, yet carbon stardust seems always to form once the temperature drops to about 1000K. The typical densities inferred for the carbon condensation zone imply that dust nucleation has to occur essentially on a collision timescale. This will form a problem for any nucleation theory. Stardust formation has generally been modeled using thermochemistry (ie., condensation sequence) and classical nucleation theory. The problems with this approach have been pointed out and it is emphasized that any theory should start by identifying the chemical pathway to dust.

The chemical processes that convert C_2H_2 into carbon stardust in the outflow from

carbon-rich giants are probably very similar to those occuring during the gas phase pyrolysis of hydrocarbon molecules in flames. PAHs may play an important role in this. Among the PAHs expected to be abundantly produced in such outflows are naphthalene, acenaphthalene, pyrene and coronene. Their detection in circumstellar shells will form an important confirmation of these chemical schemes as well as supporting the ubiquitous presence of PAHs in the interstellar medium. Photochemical processing as well as shock wave destruction will further influence the chemical composition of the *interstellar* PAH family. The carbon stardust formed in these outflows is expected to be very similar to soot and to consist of small aromatic moities (ie., PAHs) clustered in larger units and connected by aliphatic bridges and side chains (ie., tetrahedral carbon). The hydrogen content of these platelets may be very high (≈10%). These carbon platelets will be clustered in the form of larger spherical particles. The basic building blocks of carbon stardust will thus have a structure quite similar to that of hydrogenated amorphous carbon films (HAC).

The carbon stardust formation mechanism in WC 8-10 stars is not understood very well. It is likely that it starts with the formation of small acetylenic species such as C_2, C_3 and their ions. Indeed, ionization may play a dominant role. An important difference with carbon stardust formation around carbon-rich red giants is the absence of hydrogen and hydrogenated molecules in the outflow. Clearly, PAHs and HAC will not form a good model for this stardust. Actually, Buckminsterfullerene (C_{60}) and its larger analogs, formed by laser vaporization of graphite targets in a hydrogen-poor atmosphere, may play an important role in the condensation processes around these objects.

High velocity ($v \geq 7$ km s^{-1}) grain-grain collisions drive strong shock in carbon stardust which provides the high pressures required to transform some of it into diamond. This supports the suggested interstellar origin for the recently discovered small diamonds in carbonaceous meteorites by providing a feasible interstellar formation mechanism. Shock metamorphism of carbon stardust is expected to produce polycrystalline diamond grains. The microcrystalline sizes are calculated to be about 40Å, in good agreement with the measured ones in meteoritic carbon and shock experiments. Since the diamond formation is thought to go through a liquid precursor phase, the structure of the original carbon stardust grains is of little importance. Indeed, highly ordered graphite, amorphous carbon as well as glassy carbon containing substantial amounts of impurities will transform into diamonds under shock conditions.

A wide variety of isotopic anomalies have been detected in different carbon phases in carbonaceous meteorites. These carbon phases are thought to consist of interstellar or circumstellar dust grains which have been incorporated into the meteorite without major modifications. The isotopic anomalies reflect then the particular (nucleosynthetic) processes which played a role in the births sites of these grains. Among the processes that may have been important in preserving this presolar (nucleosynthetic) record in these grains are (co)condensation (eg., $^{12}C/^{13}C$; ^{14}N / ^{15}N; ^{22}Na (^{22}Ne)), ion implantation (eg., Xe HL; Q phase), and photochemical processes in the ISM (eg., D/H). Because many different sources contribute, one of the characteristics of stardust preserved in carbonaceous meteorites is a widely varying isotopic composition on a submicron scale. In particular, the $^{13}C/^{12}C$ ratio may vary dramatically on this scale depending on the source of the stardust ranging from about

zero for WC 8-10 and supernovae, solar (≈0.01) for optically visible C-rich Miras, 0.3 for some C-rich giants, to >1 for novae. In the protosolar nebula, stardust from different birthsites may have represented distinct, isotopically enriched reservoirs, which because of their different physical and chemical properties, may have been released at different times or in different parts of the nebula. Another signature of interstellar dust, which may help recognize presolar dust in meteorites or IDPs, is shock metamorphism on a submicron scale.

Acknowledgments: I thank Martin Cohen for hammering in the mystery of carbon dust formation around WC 8-10 stars during carpool hours, Helen Walker for a guided tour through the R Cr B phenomena, Mike Jura for helpful discussions on the carbon budget of the galaxy, and Stan Woosley for sharing his insight on supernova, in particular of SN 1987a. I thank Lou Allamandola and Dave Hollenbach for comments on an earlier version of this manuscript. Finally, I am indebted to Profs. E. Bussoletti and A. Borghesi for permission to show their beautiful carbon necklace.

References

1. Tielens, A.G.G.M. and Allamandola, L.J. 1987, in Interstellar Processes, eds. D.J. Hollenbach and H.J. Thronson, (Reidel, Dordrecht), p.397.
2. Tielens, A.G.G.M. and Allamandola, L.J. 1987, in Physical Processes in Interstellar Clouds, eds. G.E. Morfill and M. Scholer, (Reidel, Dordrecht), p.333.
3. Lewis, R.S., and Anders, E., 1983, Sci. Am., 249, 66.
4. Merrill, K.M. 1977, in The Interaction of Variable Stars with their Environments, eds. R. Kippenhahn, J. Rahe and W. Strohmeier, (veroff, Remeis Sternwarte, Bamberg), Bd. XI, nr 121, p446.
5. Aitken, D.K. 1981, in IAU symp. no. 96, infrared Astronomy, eds. G.C. Wynn Williams and D.P. Cruikshank (Reidel, Dordrecht), p.207.
6. Willner, S.P. 1984, in Galactic and Extragalactic Infrared Spectroscopy, eds. M.F. Kessler and J.P. Phillips, (Reidel, Dordrecht), p.37.
7. Cohen, M., Allamandola, L.J., Tielens, A.G.G.M., Bregman, J., Simpson, J.P., Witteborn, F., Wooden, D., and Rank, D., 1986, Ap. J., 302, 737,
8. Sellgren, K., Allamandola, L.J., Bregman, J., Werner, M.W., and Wooden, D., 1985, Ap.J., 299, 416.
9. Duley, W.W. and Williams, D.A., 1981, M.N.R.A.S., 196, 269.
10. Allamandola, L.J., Tielens, A.G.G.M., and Barker, J.B., 1985, Ap. J. Letters, 290, L25.
11. Leger, A., and Puget, J.L., 1984, Astr. Ap.,137, L5.
12. Barker, J.B., Allamandola, L.J., and Tielens, A.G.G.M., 1987, Ap. J. Letters, 315, L61.
13. Mathis, J.S., Rumpl, W., and Nordsieck, K.H., 1977, Ap.J., 217, 425.
14. Mathis, J.S., and Wallenhorst, S.G. 1981, Ap.J., 244, 483.
15. Greenberg, J.M., and Chlewicki,G., 1984, Ap.J.,272,563.
16. Greenberg, J.M., Hong, S.S., 1984, in Galactic Radio Astronomy, IAU symp. no. 60, eds. F.J. Kerr and S.C. Simonson, (Reidel, Dordrecht), p.155.
17. Draine, B.T., and Lee,H.M., 1984, Ap.J., 285,89.
18. Kittel, C. 1976, Introduction to Solid State Physics, (Wiley and Sons, NY).
19. Audouze, J. and Tinsley, B.M., 1976, Ann. Rev Astr. Ap., 14, 43.
20. Jura, M., 1988, elsewhere in this volume.
21. Knapp, G.R., 1987, in Late Stages of Stellar Evolution, eds. S. Kwok and S. Pottasch, (Reidel, Dordrecht), p.103.
22. Weidemann, V., and Koester, D., 1983, Astr. Ap., 121, 77.
23. Jura, M., 1987, in Interstellar Processes, eds. D.J. Hollenbach and H.J. Thronson, (Reidel,Dordrecht), p.3.

24. Thronson, H.A., Latter, W.B., Black, J.H., Bally, J., and Hacking, P., 1987, Ap.J., 322, 770.
25. Clausen, M.J., Kleinmann, S.G., Joyce, R.R., and Jura, M.,1987, Ap. J., Suppl., 65, 385.
26. Knapp, G.R., and Morris, M., 1985, Ap. J., 292, 640.
27. Knapp, G.R., and Wilcots, E.M., 1987, in Late Stages of Stellar Evolution, eds. S. Kwok and S. Pottasch, (Reidel, Dordrecht), p.171.
28. Abbott, D.C., 1982, Ap. J., 263, 723.
29. van Buren, D., 1985, Ap. J., 294, 567.
30. Truran, J. W., 1986, in Nucleosynthesis and its Implications on Nuclear and Particle Physics, eds., J. Audouze and N. Mathieu, (Reidel, Dordrecht), p.97.
31. Ferland, G.J., and Shields, G.A., 1978, Ap. J., 226, 172.
32. Gallagher, J.S., Hege, E.K., Kopriva, D.A., Williams, R.E., and Butcher, H.R., 1980, Ap. J., 237, 55.
33. Tylenda, R., 1978, Acta Astr., 28, 333.
34. Williams, R.E., Woolf, N.J., Hege, E.K., Moore, R.L., and Kopriva, D.A., 1978, Ap. J., 224,171.
35. Danzinger, I. J., 1984, in Stellar Nucleosynthesis, eds. C. Choisi and A. Renzini, (Reidel, Dordrecht), p.35.
36. Woosley, S.E., and Weaver, T.A., 1986, Ann. Rev. Astr. Ap., 24, 205.
37. Tammann, G.A., 1982, in Supernovae: A Survey of Current Research, eds. M. J. Rees and R.J. Stoneham, (Reidel, Dordrecht), p.371.
38. Woosley, S.E., 1987, private communications.
39. Thielemann, F.K., Nomoto, K., and Yokoi, K., 1986, in Nucleosynthesis and its Implications on Nuclear and Particle Physics, eds., J. Audouze and N. Mathieu, (Reidel, Dordrecht, p.131.
40. Chiosi, C., and Maeder, A., 1986, Ann. Rev. Astr. Ap., 24, 329.
41. Willis, A.J., 1982, in Wolf Rayet Stars: Observations, Physics, Evolution, eds., C.W.H. de Loore and A.J. Willis, (Reidel, Dordrecht), p.87.
42. Abbott, D.C. and Conti, P.S., 1987, Ann. Rev. Astr. Ap., 25, 113.
43. Nugis, T., 1982, in Wolf Rayet Stars: Observations, Physics, Evolution, eds., C.W.H. de Loore and A.J. Willis, (Reidel, Dordrecht), p.131.
44. Maeder, A., 1983, Astr. Ap., 120, 113.
45. Torres-Peimbert, S. and Peimbert M., in Interstellar Processes, eds. D.J. Hollenbach and H.J. Thronson, (Reidel, Dordrecht), p.667.
46. van der Hucht, K.A., Williams, P.M., and Thé, P.S., Q.J.R.A.S., 28, 254.
47. Dwek, E. et al., 1986, in Interrelationships Among Circumstellar, Interstellar, and Interplanetary Dust, ed., J.A. Nuth and R.E. Stencel, NASA CP 2403, WG-1.
48. Gehrz, R.D., Ney, E.P., Grasdalen, G.L., Hackwell, J.A., and Thronson, H.A., 1984, Ap. J., 281, 303.
49. Knapp, G.R., and Chang, K.M., 1985, Ap. J., 293, 281.
50. Zuckerman, B., 1980, Ann. Rev. Astr. Ap., 18, 263.
51. Audouze, J., and Lazareff, B., 1977, in Novae and Related Stars, ed. M. Friedjung, (Reidel, Dordrecht), p.205.
52. Starrfield, S., Sparks, W.M., and Truran, J.W., 1985, Ap.J., 291, 136.
53. Wiescher, M., Gorres, J., Thielemann, F.K., and Ritter, H., 1986, in Nucleosynthesis and its Implications on Nuclear and Particle Physics, eds., J. Audouze and N. Mathieu, (Reidel, Dordrecht), p.105.
54. Hawkins, and Jura, M., 1987, Ap. J., 317, 374.
55. Hawkins, I., 1987, private communications.
56. Jura, M., 1987, private communications.
57. Pagel, B.E.J., and Edmunds, M.G., 1981, Ann. Rev. Astr. Ap., 19, 77.
58. Martin, P.G., and Rogers, C., 1987, Ap. J., 322, 374.
59. Lambert, D.L.,1986, in Hydrogen Deficient Stars and Related Objects, ed. K. Hunger, (Reidel, Dordrecht), p.127.
60. Lambert, D.L., 1987, in Astrochemistry, eds., M.S. Vardya and S.P. Tarafdar, (Reidel,

Dordrecht), p.583.
61. Omont, A., 1987, in Astrochemistry, eds., M.S. Vardya and S.P. Tarafdar, (Reidel, Dordrecht), p.357.
62. Feast, M.W.,1986, in Hydrogen Deficient Stars and Related Objects, ed. K. Hunger, (Reidel, Dordrecht), p.151.
63. Tsuji, T., 1987, in Astrochemistry, eds., M.S. Vardya and S.P. Tarafdar, (Reidel, Dordrecht), p.409.
64. Williams, P.M., van der Hucht, K.A., and Thé, P.S., 1987, Astr. Ap., 182, 91.
65. Querci, F., and Querci, M., 1974, in Highlights of Astronomy, 3, 341.
66. Warner, 1967, M.N.R.A.S., 137, 119.
67. Lambert, D.L., Gustafsson, B., Erickson, K., and Hinkle, K.H., 1986, Ap.J. Suppl., 62, 373.
68. Iben, I., 1987, in Late Stages of Stellar Evolution, eds., S. Kwok and S.R. Pottasch, (Reidel, Dordrecht), p175.
69. Renzini, A., 1982, in Wolf Rayet Stars: Observations, Physics, Evolution, eds., C.W.H. de Loore and A.J. Willis, (Reidel, Dordrecht), p.413.
70. Fadeyef, Y.A., 1986, in Hydrogen Deficient Stars and Related Objects, ed. K. Hunger, (Reidel, Dordrecht), p.441.
71. Salpeter, E.E., 1974, Ap. J., 193, 579.
72. Tielens,A.G.G.M., 1983, Ap.J., 271, 702.
73. Betz, A., 1987, in Astrochemistry, eds., M.S. Vardya and S.P. Tarafdar, (Reidel, Dordrecht), p.327.
74. Olofson, H., 1987, in Late Stages of Stellar Evolution, eds., S. Kwok and S.R. Pottasch, (Reidel, Dordrecht), p.149.
75. Cernicharo, J., Guelin, M., Menten, K.M., and Walmsley, C.M., 1987, Astr. Ap., 181, L1.
76. Cernicharo, J., Guelin, M., Hein, H., and Kahane, C., 1987, Astr. Ap., 181, L9.
77. Tarafdar, S.P., 1987, in Astrochemistry, eds., M.S. Vardya and S.P. Tarafdar, (Reidel, Dordrecht), p.559
78. Gail, H.P., and Sedlmayr, E., 1987, in Physical Processes in Interstellar Clouds, eds. G.E. Morfill and M. Scholer, (Reidel, Dordrecht), p.275.
79. Frenklach, M., elsewhere in this volume.
80. Salpeter, E.E., 1977, Ann. Rev. Astr. Ap., 15, 267.
81. Grossman, L., and Larimer, J.W., 1974, Rev. Geophys. Space Phys., 12, 71.
82. Barshay, S.S. and Lewis, J.S., 1976, Ann. Rev. Astr. Ap., 14, 81.
83. Draine, B.T., 1986, in Interrelationships Among Circumstellar, Interstellar, and Interplanetary Dust, ed., J.A. Nuth and R.E. Stencel, NASA CP 2403, 19.
84. Draine, B.T., 1979, Astr. Space Sci., 65,313.
85. Donn, B, and Nuth, J., 1985, Ap.J., 288, 187.
86. Nuth, J., 1987, Nature, 329, 589.
87. Donn, B., 1978 in Protostars and Planets, ed. T. Gehrels, (Univ. of Arizona Press, Tucson), p.100.
88. Keller, R., 1987, in Polycyclic Aromatic Hydrocarbons and Astrophysics, eds., A. Leger, L.B. d'Hendecourt, and N. Bocarra, (Reidel, Dordrecht), p. 387.
89. Hucknall, D.J., 1985, Chemistry of Hydrocarbon Combustion, (Chapman and Hall, New York).
90. Barnard, J.A., and Bradley, J.N., 1985, Flame and Combustion, (Chapman and Hall, New York).
91. Smyth, K.C., and Miller, J.H., 1987, Science, 236, 1540.
92. Bussoletti, E., Colangeli, L., Borghesi, A., 1987, in Polycyclic Aromatic Hydrocarbons and Astrophysics, eds., A. Leger, L.B. d'Hendecourt, and N. Bocarra, (Reidel, Dordrecht), p. 63.
93. Borghesi, A., Bussoletti, E., and Colangeli, L., 1985, Astr. Ap., 142, 225.
94. Koike, C., Hasegawa, H., and Manabe, A., 1980, Ap. Space Sci., 67, 495.
95. Palmer, H.B., and Cullis, C.F., 1965, in Chemistry and Physics of Carbon vol.1, ed., J. Walker, (Marcel Dekker, New York), p.265.
96. Smalley, 1988, elsewhere in this volume.
97. Kroto, H., 1988, elsewhere in this volume.

98. Homann, K.H., 1984, in Twentieth Symp. (Int.) on Combustion, 857.
99. Willson, L.A., and Hill, S.J., 1979, Ap.J., 228, 854.
100. Wood, P.R., 1979, Ap.J., 227,220.
101. Willson,L.A., 1987, in Late Stages of Stellar Evolution, eds., S. Kwok and S.R. Pottasch, (Reidel, Dordrecht), p.253.
102. Bowen and Beach, 1987, in Late Stages of Stellar Evolution, eds., S. Kwok and S.R. Pottasch, (Reidel, Dordrecht), p.275.
103. Frenklach, M., Clary, D.W., Gardiner, W.C., and Stein, S.E., 1984, in Twentieth Symp. (Int.) on Combustion, 887.
104. Bockhorn, H., Fetting, F., and Wenz, H.W., 1983, Ber. Buns. Phys. Chem., 87, 1067.
105. Stein, S.E., 1978, J. Phys. Chem., 82, 566.
106. Kroto, H.W., Heath, J.R., O'Brien, S.C., Curl, R.F., and Smalley, R.E., 1985, Nature, 318, 162.
107. Crawford, M.K., Tielens, A.G.G.M., Allamandola, L.J., 1985, Ap.J. Letters, 293, L45.
108. Allamandola, L.J., Tielens, A.G.G.M., and Barker, J.R., in in Physical Processes in Interstellar Clouds, eds. G.E. Morfill and M. Scholer, (Reidel, Dordrecht), p.305.
109. Goldreich, P., and Scoville, N., 1976, Ap.J., 205,144.
110. Clegg, R.S., and Wootten, A., 1980, Ap. J., 240, 828.
111. Calcote, H.F., 1981, Comb. Flame, 42, 215.
112. Cohen, M., et al. 1988, in preparation.
113. Kerridge, J.F., elsewhere in this volume.
114. Woosley, S.E., Pinto, P.A., and Ensman, L., 1987, Ap. J., 324, 466.
115. Woosley, S.E., 1987, preprint.
116. Kirshner, R.P., 1987, IAU colloq. 108, in press.
117. Lattimer, J.M., Schramm, D.N., and Grossman, L., Ap. J., 219, 230.
118. Draine, B.T., and Salpeter, E.E., 1979, Ap.J., 231, 438.
119. Shull, J.M., 1978, Ap.J., 226, 858.
120. Seab, C.G., and Shull, J.M., 1983, Ap. J., 275, 652.
121. Seab, C.G., 1987, in Interstellar Processes, eds., D.J. Hollenbach and H.J. Thronson, (Reidel, Dordrecht), p.491; and elsewhere in this volume.
122. Routly, P.M., and Spitzer, L., 1952, Ap. J., 115, 227.
123. Cowie, L.L., 1978, Ap. J., 225, 887.
124. Lewis, R.S., Tang, M., Wacker, J.F., Anders, E., and Steel, E., 1987, Nature, 326, 160.
125. Tielens, A.G.G.M., Seab, C.G., Hollenbach, D.J., and McKee, C.F., 1987, Ap.J. Letters, 319, L109.
126. Rae, W.J., 1970, in High Velocity Impact Phenomena, ed. R. Kinslow, (Acad. Press, New York), p.214.
127. Tielens, A.G.G.M., McKee, C.F., Seab, C.G., and Hollenbach, D.J., 1988, in preparation.
128. Zel'dovich, Ya.B., and Raizer, Yu.P., 1966, Physics of Shock Waves and High Temperature Hydrodynamic Phenomena, vol 2, (Acad. Press, New York).
129. McKee, C.F., Hollenbach, D., Seab, C.G., and Tielens A.G.G.M., 1987, Ap. J., 318, 674.
130. De Carli, P.S., and Jamieson, 1961, Science, 133, 1821.
131. Alder, B.J., and Christian, R.H., 1961, Phys. Rev. Lett., 7, 367.
132. McQueen, R.G., and Marsh, S.P., 1968, in Behavior of Dense Media under High Dynamic Pressures, (Gordon and Breach, New York), p207.
133. Pavlovskii, M.N., Sov. Phys. Solid State, 13, 741.
134. Gust, W.H., and Young D.A., 1979, in High Pressure Science and Technology, vol I, eds. K.D. Timmerhaus and M.S. Barter, (Plenum Press, New York), p944.
135. De Carli, P.S., 1979, in High Pressure Science and Technology, vol I, eds. K.D. Timmerhaus and M.S. Barter, (Plenum Press, New York), p940.
136. Bundy, F.P., 1985, Solid State Physics under Pressure, ed., S. Minomura, (Terra Sci. Publ. Co.), p.1.
137. Gold, J.S., Bassett, W., Weathers, M.S., and Bird, J.M., 1984, Science, 225, 921.

138. Young, D.A. and Grover, R., 1988, preprint.
139. Yin, M.T., and Cohen, M.L., 1983, Phys. Rev. Letters, 50, 2006.
140. Whittaker, A.G., 1978, Science, 200, 763.
141. Whittaker, A.G., Watts, E.J., Lewis, R.S., and Anders, E., 1982, Science, 209, 1512.
142. Heimann, R.B., Kleiman, J., and Slansky, N.M., 1983, Nature, 306, 164.
143. Smith, P.P.K. and Buseck, P.R., 1982, Science 216, 984.
144. Shaner, J.W., Brown, J.M., Swenson, C.A., and McQueen, R.G.,1984, J. Phys., C8, 235.
145. Bergmann, O.R., 1983, in Shock Waves in Condensed Matter, eds., J.R. Asay, R.A. Graham, and G.K. Straub, (Elsevier, Amsterdam), p.429.
146. Bundy, F.P., Strong, H.M., and Wentorf, R.H., 1973, in Chemistry and Physics of Carbon, 10, eds. P.L. Walker and P.A. Thrower, (M. Dekker, New York), p213.
147. Turro, N.J., 1978, Modern Molecular Photochemistry, (Benjamin/Cummins, Menlo Park).
148. Frank, F.C., 1952, Proc. Roy. Soc. London, Ser. A, 215, 43.
149. Bernal, J.D., 1960, Nature, 185, 68.
150. Anderson, J,F., 1975, Structure of Metalic Catalysts, (Acad. Press, New York).
151. Nelson, D.R., 1983, Phys. Rev. B, 28, 5515.
152. Galvin, G.J., Thompson, M.O., Mayer, J.W., Hammond, R.B., Poulter, N., Peercy, P.C., 1982, Phys. Rev. Letters, 48,33.
153. Berman, R., 1979, The Properties of Diamonds, ed. J.E. Field (Acad. Press, New York), p.3.
154. Dienes, J.K., and Walsh, J.M., 1970, in High Velocity Impact Phenomena, ed. R. Kinslow, (Acad. Press, New York), p46.
155. Trueb, L.F., 1968, J. Appl. Phys., 39, 4707.
156. Blake, D., Freund, F., Krishnan, K., Echer, C., Sipp, R., Bunch, T., Tielens, A., Lipari, R.J., Hetherington, C. and Chang, S., 1988, Nature in press.
157. Griffith, A.A., 1920, Phil. Trans. R. Soc., A221, 163.
158. Kendall, K., 1978, Nature, 272, 710.
159. Ruoff, A.L., 1979, 1979, in High Pressure Science and Technology, vol I, eds. K.D. Timmerhaus and M.S. Barter, (Plenum Press, New York), p.525..
160. Gigl, P.D., 1979, 1979, in High Pressure Science and Technology, vol I, eds. K.D. Timmerhaus and M.S. Barter, (Plenum Press, New York), p915.
161. Gault, D.E. and Wedekind, J.A., 1969, J. GeoPhys. Res., 74, 6780.
162. Matsui, T., Waza, T., Kani, K., and Suzuki, S., 1982, J. Geophys. Res., 87, B10,968.
163. Takagi, Y.,Mizutani, H., and Kawakami, S., 1984, Icarus, 59, 462.
164. Bibby, D.M., 1982, in Chemistry and Physics of Carbon,18, ed. P.A. Thrower, (Dekker, New York), p1.
165. Setaka, N., and Sekikawa, Y., 1981, J. Mat. Sci., 16,1728.
166. Ree, F.H., Nellis, W.J., Trainor, R.J., Mitchell, A.C., and Boslough, M.B., 1983, in Shock Waves in Condensed Matter, eds., J.R. Asay, R.A. Graham, and G.K. Straub, (Elsevier, Amsterdam), p.42.
167. Wentorf, R.H., 1965, J. Phys. Chem., 69, 3063.
168. Bundy, F.P., 1963, J. Chem. Phys., 38, 618.
169. Appleton, B.R., and Celler, G.K., 1982, Laser and Electron Beam Interaction with Solids, (Elsevier, Amsterdam).
170. Landau, R., 1970, Nature, 226, 924.
171. Allamandola, L.J., 1987, in Polycyclic Aromatic Hydrocarbons and Astrophysics, eds. A. Leger, L.B. d'Hendecourt, and N. Bocarra, (Reidel, Dordrecht), p339.
172. Kerridge, J.F., and Chang, S., 1986, in Protostars and Planets II, eds. D.C. Black and M. Mathews, (Univ. Arizona Press, Tucson), p.738.
173. Maeder, A., 1983, Astr. Ap., 120, 130.
174. Clayton, D.D., Nature, 257, 36.
175. Herold, A., in Intercalated Layered Materials, ed. F. Levy, (Reidel, Dordrecht), p. 321.
176. Renzini, A., 1984, in in Stellar Nucleosynthesis, eds. C. Chiosi and A. Renzini, (Reidel, Dordrecht), p.99.

177. Clayton, D.D., 1981, Proc. Lun. Plan. Sci. Conf., 12B, 1781.
178. Watson, W.D., 1976, in Atomic and Molecular Physics and the Interstellar Matter, eds. R. Balian, P. Encrenaz, and J. Lequeux, (Elsevier, Amsterdam), p.177.
179. Tielens, A.G.G.M., 1983, Astron. Astr. , 119, 177.
180. Geiss, J., and Reeves, H. 1981, Astron. Astr., 93,189.
181. Allamandola, L.J., Tielens, A.G.G.M., and Barker, J.B., 1988, in preparation.
182. d'Hendecourt, L.B., Allamandola, L.J., Grim, R.J.A., and Greenberg J.M., 1986, Astron. Astr., 158, 119.
183. Agarwal,V.K., Schutte, W., Greenberg, J.M., Ferris, J.P., Briggs, R., Connor, S., van de Bult, C.E.P.M., and Baas, F., 1985, Origins of Life, 16, 21.